Long-distance entanglement sharing using hybrid states of discrete and continuous variables

Soumyakanti Bose,[1,*] Jaskaran Singh,[2,3,†] Adán Cabello,[2,4,‡] and Hyunseok Jeong[1,§]

[1] *Department of Physics & Astronomy, Seoul National University, Gwanak-ro 1, Gwanak-gu, 08826 Seoul, Korea*

[2] *Departamento de Física Aplicada II, Universidad de Sevilla, 41012 Seville, Spain*

[3] *Department of Physics and Center for Quantum Frontiers of Research and Technology (QFort), National Cheng Kung University, Tainan 701, Taiwan*

[4] *Instituto Carlos I de Física Teórica y Computacional, Universidad de Sevilla, 41012 Seville, Spain*

(Received 19 June 2023; revised 2 April 2024; accepted 10 May 2024; published 6 June 2024)

We introduce a feasible scheme to produce high-rate long-distance entanglement that uses hybrid entanglement between continuous variables (CVs) and discrete variables (DVs). We show that hybrid entanglement can effectively remove the experimental limitations of existing CV and DV systems to produce long-range entanglement. We benchmark the resulting DV entangled states using an entanglement-based-quantum-key-distribution protocol. We show, using hybrid entangled states, that entanglement-based quantum key distribution is possible with standard telecommunication fibers for 300 km. The key idea is the use of the CV part, which can be adjusted to be robust regarding photon losses, for increasing the transmission distance, and the use of the DV part for achieving high secure key rates. Our results show that hybrid entangled states provide a clear advantage for practical generation of long-distance and high-rate entanglement that may lead to further applications in quantum information processing.

DOI: 10.1103/PhysRevApplied.21.064013

I. INTRODUCTION

Generation of high-rate entanglement between distant locations is crucial for fundamental tests of quantum theory and many applications. For example, it is needed for extending the current distances and rates of loophole-free Bell tests [1,2], quantum steering [3], and quantum teleportation [4], which so far are feasible only for relatively short ranges. It is also needed for increasing the transmission distance and the key rate of entanglement-based-quantum-key-distribution (EBQKD) protocols, most notably device-independent QKD [5–7], which currently suffers from both these issues. Moreover, higher rates in distant locations will also allow us to achieve higher detection efficiencies (which are needed both for loophole-free Bell tests and device-independent QKD) by means of heralded qubit amplifiers [8] or photonic precertification schemes [9–11], whose practicality is currently limited by the rates achieved after transmission.

A benchmark of high-rate entanglement over long distances, from an operational perspective, can be set by its performance in an information-processing task such as an EBQKD protocol. These protocols can be broadly classified into two distinct classes: (1) those using discrete-variable (DV) entangled states and (2) those that use continuous-variable (CV) entangled states, where each class has its own set of advantages and limitations [12–14]. As an example, DV EBQKD protocols offer composable security proofs with good key rate, but they require precise Bell-state or single-photon measurements at extremely low temperatures, which are hard to perform even in laboratory conditions. On the other hand, CV EBQKD protocols generally require Gaussian states, which are comparatively easier to prepare, but their performance is limited by the requirement of almost-ideal homodyne detectors at telecommunication wavelengths [13,15,16]. As a consequence, despite extensive theoretical and experimental analysis of both types of system, the quest for an optimal physical system that can be potentially used to share high-rate entanglement remains open.

Nonetheless, there exists a different class of physical systems where the entanglement is between CV and DV systems and that are formally known as hybrid entangled (HE) states [17–22]. These strongly correlated [23–25] cross-system entangled states play a crucial role in various quantum information processing tasks, including quantum computation, communication, and tests of Bell

*Corresponding author: soumyakanti.bose09@gmail.com
†Corresponding author: jaskaran@us.es
‡Corresponding author: adan@us.es
§Corresponding author: h.jeong37@gmail.com

nonlocality [25–33], and have been efficiently generated in a wide range of experimental setups [34–38]. Consequently, it is interesting to observe whether such hybrid states can be used to share entanglement among distant locations without the limitations faced by CV and DV systems.

Here we propose a scheme based on HE states as an initial resource that produces high-rate DV entanglement between locations that are extremely far apart. We provide a characterization of such states and show that it is possible to share entanglement between locations that are hundreds of kilometers apart. We further assess the quality of shared entanglement in the context of EBQKD. We show that, by bringing out the best of CV and DV systems, with HE states, it is possible to achieve secure key rate at a distance of 300 km by the use of practical homodyne detectors with efficiency $\eta_h = 0.55$ [39–43] (which is a reasonable value at telecommunication wavelengths [40]) and ON-OFF detectors with efficiency $\eta_0 = 0.8$ [44]. Note that we use the key rates and transmission distances only to quantify the quality of the entanglement; our central goal is to show the advantage of the use of HE states to achieve entanglement over longer distances, which is a crucial tool enabling a wide range of fundamental tests in physics and quantum information processing applications.

Our scheme hinges on generating a single-photon DV entangled state between two distant parties by exploiting CV entanglement swapping [33] by a third party located midway. It offers three major advantages as compared with earlier CV and DV EBQKD protocols: (1) elimination of major limiting factors of DV EBQKD, which include high-precision Bell-state or single-photon measurements as well as the photon-number-splitting attack by an eavesdropper by considering entanglement swapping over the CV system; (2) elimination of the requirement of near-unit efficiency for the homodyne detectors used for key generation in CV EBQKD;(3) long transmission distance at telecommunication wavelengths stemming from the robustness of the multiphoton coherent state regarding transmission losses and the use of practical devices.

This article is organized as follows. In Sec. II, we provide a brief introduction to HE states. We then propose a protocol to share DV entanglement among distant locations by using HE states as an initial resource. We also characterize the resulting entanglement using logarithmic negativity and show that it can be nonzero even when the parties are hundreds of kilometers apart. In Sec. III, we benchmark the usefulness of the resultant entangled states by demonstrating our scheme as an EBQKD protocol using practical devices. In Sec. IV, we discuss our results by arguing that our protocol provides a practical solution to the problem of long-distance-entanglement generation, which is a central requirement in several information-processing tasks.

II. ENTANGLEMENT SHARING WITH HYBRID STATES

In this section we first provide a brief description of HE states. Subsequently, we detail our protocol to share long-distance entanglement using these states.

A. Hybrid entangled states

Let $|0\rangle$ and $|1\rangle$ correspond to photon-number states in the Fock basis and let $|\alpha\rangle$ correspond to a coherent state of quantized light with coherent amplitude α. For the remainder of this paper, we represent the number of photons as a DV system, while the coherent state represents a CV system. We define an HE state as an entangled pair, where the entanglement is between the DV and CV degrees of freedom. Mathematically, such HE states can be written as

$$|\psi\rangle_{a_1a_2} = \frac{1}{\sqrt{2}}\left(|0\rangle_{a_1}|\alpha\rangle_{a_2} + |1\rangle_{a_1}|-\alpha\rangle_{a_2}\right), \qquad (1)$$

where a_1 and a_2 are the two modes pertaining to the DV and CV parts, respectively.

We stress that HE states with small coherent amplitudes ($\alpha \lesssim 1$) are experimentally available. They have been generated experimentally in various settings, such as conditional photon subtraction on a coherent state [34] as well as photon subtraction on two squeezed states [35] (see Appendix A for further details). While these techniques produce HE states with nonunit probability, it should be noted that typical methods to generate standard entangled photon pairs, e.g., parametric down-conversion, also do so nondeterministically. In Fig. 1(b), we show the linear optics–based schematic for generating HE states as originally described in Ref. [34].

B. Protocol for entanglement sharing

We consider two distant parties, Alice and Bob, each of them having access to bipartite HE states $|\psi\rangle_{a_1a_2}$ and $|\psi\rangle_{b_1b_2}$ given by Eq. (1). We consider these as initial resource states that will be used to share a DV entangled state between the parties. We provide a step-by-step description of the protocol, schematically represented in Fig. 1(a), while a detailed mathematical calculation can be found in Appendix B.

Step 1: Alice and Bob generate HE states $|\psi\rangle_{a_1a_2}$ and $|\psi\rangle_{b_1b_2}$ in their respective laboratories. Both parties transmit the CV part of their systems, corresponding to modes a_2 and b_2, respectively, to a third, untrusted party, Charlie, who lies midway between them, through a lossy quantum channel with transmittance T ($0 \leq T \leq 1$). Additionally, Bob also transmits the state $|\sqrt{2}\alpha\rangle$ to Charlie separately through a similar quantum channel. After passing through channels with transmission losses, Charlie receives mode a_2 from Alice, mode b_2 from Bob, and the additional state

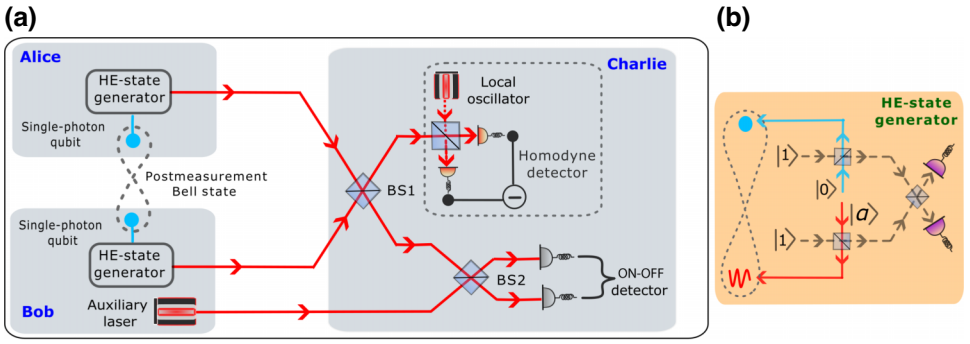

FIG. 1. (a) Scheme for generating DV entangled states between Alice and Bob using HE states. The DV part (cyan) and the CV part (red) of the HE state stand for the single-photon state and the coherent state, respectively. Alice and Bob send the CV part of their individual HE states to Charlie, who then mixes the incoming signals at a balanced beam splitter (BS1) and uses one of the output modes for homodyne measurement with efficiency η_h. The other outgoing signal of BS1 is used for a postselection measurement by ON-OFF detectors with efficiency η_0, after it has been mixed at another balanced BS (BS2) with the additional coherent signal sent by Bob. Upon declaration of the results by Charlie, Alice and Bob obtain a DV entangled pair that is used for secure key generation. (b) Scheme for generating HE states. Two auxiliary single photons (dashed gray line) are mixed with vacuum and coherent states at the two BSs. The outgoing auxiliary photons are then mixed with each other at a second BS. When the detector placed at the output of the second BS clicks, the HE state between the single-photon state and the coherent state is obtained.

$|\sqrt{2T}\alpha\rangle$ from Bob, which we label as mode c. While a general quantum channel between the parties will comprise both transmission loss and thermal noise, here, for simplicity, we consider only lossy quantum channels with no noise. In Appendix F 4 we demonstrate that the scenario involving a practical level of thermal noise closely matches our current findings.

The effect of a quantum state passing through a noisy channel can be seen as the system undergoing photon loss. In Fig. 2, we plot the logarithmic negativity of the HE state when its CV part undergoes photon loss as a function of the coherent amplitude α (see Appendix C for details). We find that there exists an optimal value of α for a fixed

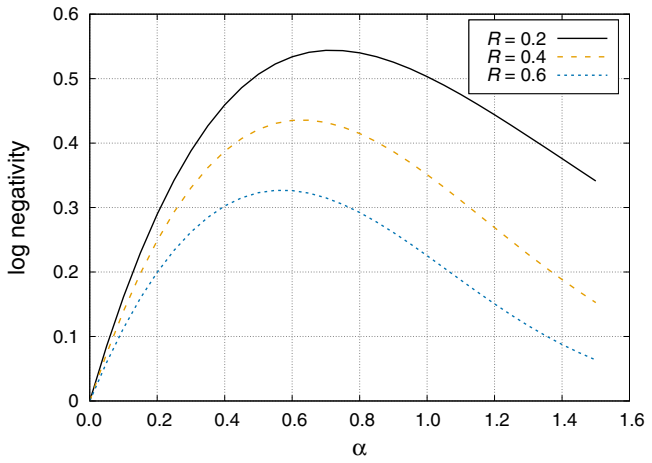

FIG. 2. Logarithmic negativity of the HE state undergoing photon loss over the CV part as a function of the coherent amplitude α. R $(0 \leq R \leq 1)$ stands for the normalized strength of loss.

value of photon loss. We denote the photon-loss fraction by R, such that $R = 0$ and $R = 1$ correspond to no photon loss and complete photon loss, respectively. For a significantly lossy channel, we find that the optimal value of α approaches 0.5. This value becomes important when we benchmark the resultant DV entangled state by a EBQKD protocol.

This behavior of HE states can be qualitatively understood in terms of the interplay between entanglement and the fragility of the initial HE state. Starting from the initial separable state at $\alpha = 0$, the HE state becomes more entangled as α increases. An increase in α also corresponds to an increase in the average number of photons, which can be understood as an increase in the mean energy of the system. However, with an increase in the mean energy, the state becomes more vulnerable to decoherence. This behavior is similar to what is also shown in Ref. [45] for superposition of coherent states, and the advantage of using small amplitudes under photon losses was demonstrated in the context of teleportation [46]. As a consequence, with increase in α beyond an optimal value, the HE state becomes extremely fragile under noise, leading to a drop in entanglement when the multiphoton part passes through a noisy quantum channel.

Step 2: Next, Charlie mixes the two incoming modes a_2 and b_2 via a beam splitter (BS), labeled as "BS1" in Fig. 1, with two output modes, which we label as a_2' and b_2'. In our protocol we are specifically interested in the vacuum-state contributions from mode a_2'. To extract this contribution, Charlie mixes this mode though a second BS (BS2) with mode c with output modes labeled a_2'' and c'. Charlie now performs a projective measurement, $\mathcal{M} = \{\Pi_0, \mathbb{1} - \Pi_0\}$, where $\Pi_0 = (\mathbb{1} - |0\rangle\langle 0|)_{a_2''} \otimes (\mathbb{1} - |0\rangle\langle 0|)_{c'}$. This measurement is accomplished by the

use of ON-OFF detectors (which detect only the presence of photons) on each of the modes a_2'' and c'. Charlie then publicly announces the outcome of the projective measurement, which is considered to be successful only if the result Π_0 is obtained, i.e., both detectors click. In that case, the protocol continues. Otherwise, the measurement is deemed unsuccessful and the parties must repeat the aforementioned steps. To model realistic detectors, we consider imperfect ON-OFF detectors with efficiency η_0.

Step 3: After a successful projective measurement (as dictated in step 2), Charlie performs a homodyne measurement on mode b_2' and, again, announces the results publicly. We consider that homodyne measurements have efficiency η_h.

Step 4: After a public announcement of the results of a successful projective measurement and the homodyne measurement by Charlie, Alice and Bob end up with the final normalized single-photon Bellstate in modes a_1 and b_1 as

$$\rho_{a_1b_1} = \frac{1}{2}\Big[\,|01\rangle\langle 01| + |10\rangle\langle 10| + h\left(g\,|01\rangle\langle 10| + g^*\,|10\rangle\langle 01|\right)\Big], \quad (2)$$

with probability

$$P_0 = \frac{\left(1 - e^{-\eta_o T\alpha^2}\right)^2}{2}, \quad (3)$$

where $h = e^{-4(1-T\eta_h)\alpha^2}$, $g = e^{4i\sqrt{T\eta_h}\alpha p}$, g^* is the conjugate of g, and p is the result of the homodyne measurement.

C. Shared DV entanglement between the parties

The entanglement of the final DV entangled state shared between the parties depends on a number of parameters. However, the quantities of most interest are the transmission length and the coherent amplitude.

In Fig. 3, we plot the logarithmic negativity of the state $\rho_{a_1b_1}$ as a function of the transmission distance for different values of the coherent amplitude α. We assume that the transmittance of the channels is given by T_A and T_B, respectively, such that $T_A = 10^{-l(L_{AC}/10)}$ and $T_B = 10^{-l(L_{BC}/10)}$, where $l = 0.2$ dB/km is the standard channel loss for telecommunication wavelengths [47,48] and L_{AC} and L_{BC} are the transmission distances between Alice and Charlie and between Bob and Charlie, respectively. To simplify the scenario, we also assume that Charlie is midway between Alice and Bob such that $L_{AC} = L_{BC} = L/2$, where L is the total transmission distance. We find that the entanglement of the final state decreases exponentially with the total transmission distance. As an example, at $L = 100$ km, the logarithmic negativity is 1.3×10^{-4} for coherent amplitude $\alpha = 0.6$ (see Appendix D for further detail).

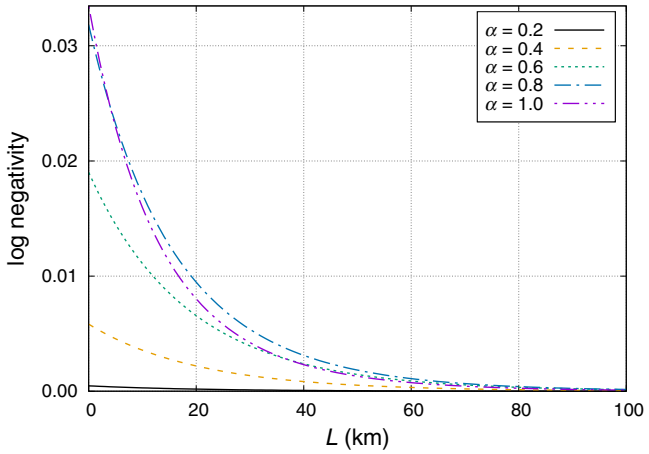

FIG. 3. Logarithmic negativity of the state $\rho_{a_1b_1}$ as a function of the transmission distance L for different values of coherent amplitude α. We assume detection efficiencies $\eta_h = 0.55$ for the homodyne detectors and $\eta_0 = 0.8$ for the ON-OFF detectors, and $p = \pi/2$.

In Fig. 4, we plot the logarithmic negativity as a function of the coherent amplitude α for different transmission distances. It is evident from Fig. 4 that the shared entanglement varies nonmonotonically with the coherent amplitude (α). We observe that as the transmission distance increases, the optimal value of α becomes less than unity. For greater transmission distance ($L \geq 150$ km), this optimal value becomes close to 0.5 (not shown in Fig. 4). It is found that there also exists an optimal value of α that offers maximum entanglement at a given distance that may be different from the optimal value of α that maximizes the entanglement of the original HE state (as shown in Fig. 2).

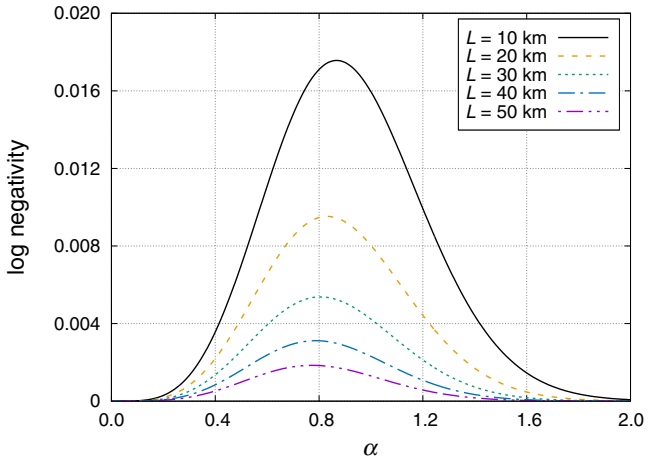

FIG. 4. Logarithmic negativity of the state $\rho_{a_1b_1}$ as a function of the transmission distance (L) for different values of coherent amplitude α. We assume detection efficiencies $\eta_h = 0.55$ for the homodyne detectors and $\eta_0 = 0.8$ for the ON-OFF detectors, and $p = \pi/2$.

III. QUANTUM KEY DISTRIBUTION USING HE STATES

In this section we benchmark the quality of the shared entangled state in terms of an EBQKD protocol that we set up in accordance with the scheme presented in Sec. II B. We also consider an eavesdropper, Eve, who may collaborate with Charlie to determine the secure key that is being shared between Alice and Bob. Additionally, in our protocol we make the following assumptions:

(1) We assume that Alice and Bob have access to secure laboratories in which they can perform well-characterized measurements. Moreover, the measurement devices of Alice and Bob are assumed to be immune to any side-channel attack since no unwanted system may enter or exit the secure laboratories. In the protocol, the DV modes a_1 and b_1 with Alice and Bob, respectively, are assumed to be in these secure laboratories and do not directly take part in the transmission. On the other hand, the CV modes a_2 and b_2 are not assumed to be in secure laboratories and therefore they are vulnerable to eavesdropping attacks.

(2) We also assume that the quantum channels between Alice and Charlie and between Bob and Charlie are characterized by transmission losses only, with no thermal noise. We justify this assumption by demonstrating, in Appendix F 4, that the scenario with no thermal noise approximates the scenario with some practical value of the thermal noise with more than 98% fidelity. This assumption is required only to manage the calculation complexity of evaluating the final DV state between Alice and Bob.

(3) We also consider a third party, Charlie, who is assumed to be untrusted and can collaborate with an eavesdropper, Eve. In the worst-case scenario, we assume that he is identified as Eve herself. The QKD protocol, as described in Sec. II B, dictates that Charlie performs certain measurements and publicly declares the outcomes so that Alice and Bob can share an entangled state. In principle, we assume that Charlie, as an eavesdropper, may not perform the operations as dictated by the protocol. However, it is required for him to supply some outcomes of the specified measurements to activate the correlations between Alice and Bob. However, if these outcomes are tampered with or even fabricated, the correlations between Alice and Bob will decrease. It is then possible for Alice and Bob to detect the presence of Eve by various methods, including state tomography, since the parties know the final state they should potentially share. More details on this assumption and the concept of secure laboratories can be found in Ref. [49].

A. Steps in evaluating the key rate

It should be noted that the steps of the QKD protocol directly follow after step 4 in Sec. II B as

Step 5: For the case in which Alice and Bob share $\rho_{a_1b_1}$, they perform two-outcome measurements $\mathcal{M}_A$ and $\mathcal{M}_B$ on their respective subsystems to generate a raw key. The choice of measurements is made before the protocol is started and the information about this choice is usually publicly available. In our protocol, they perform Pauli measurements corresponding to σ_Z on their respective subsystems to generate a raw key. The length of the raw key that the parties can generate is quantified by the mutual information $I(A:B)$ between them for the observable σ_Z.

Step 6: Alice and Bob then estimate the amount of information that an adversary, Eve, can have on their raw key. This information is quantified by the Holevo bound $\chi(A:E)$ between Alice and Eve. In our protocol we consider the Holevo bound to quantify the knowledge of the coherent amplitude α and the results of the ON-OFF and homodyne measurements. These parameters are publicly declared and actively used in generating the final state between Alice and Bob. These results can be used by Eve and therefore must be taken care of in the security analysis.

B. Simulation results on the secured key rate

Our protocol comprises two quantum channels: one between Alice and Charlie and another between Bob and Charlie. As before, we consider that the transmittance of the channels is given by T_A and T_B, respectively, such that $T_A = 10^{-l(L_{AC}/10)}$ and $T_B = 10^{-l(L_{BC}/10)}$, where $l = 0.2$ dB/km is the standard channel loss for telecommunication wavelengths [47,48] and $L_{AC} = L_{BC} = L/2$ are the transmission distances between Alice and Charlie and between Bob and Charlie, respectively, where L is the total transmission distance.

Moreover, we consider that the detectors of Alice and Bob have efficiency η_d such that the error rate is given as $Q = 1 - \eta_d$. With these inefficient detectors, the final secure key rate (see Appendix E for a detailed analysis) for the state given in Eq. (2) is given as

$$\begin{aligned} r &\geq P_0\,[I(A:B) - \chi(A:E)] \\ &= P_0 \Big\{ 1 - \eta_d + \frac{1}{2}\big[(1+h)\log_2(1+h) \\ &\quad + (1-h)\log_2(1-h)\big] - \frac{1}{2}\big[(2-\eta_d)\log_2(2-\eta_d) \\ &\quad - (1-\eta_d)\log_2(1-\eta_d)\big] \Big\}, \end{aligned} \tag{4}$$

where it can be seen that the secure key rate depends only on h [from Eq. (2)], the efficiency of the detectors of of Alice and Bob, and the probability with which the final state is prepared.

Generally, for an experimental realization of the QKD protocol, the laboratories of Alice and Bob are fixed at some distance L. We show that α cannot be chosen

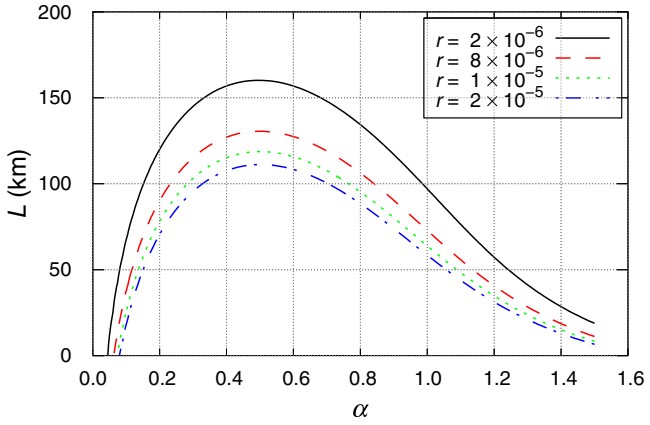

FIG. 5. Total transmission distance as a function of the coherent amplitude for different values of the secure key rate. We fix the channel loss at $l = 0.2$ dB/km, which corresponds to losses in standard optical fibers. We also fix $\eta_d = 0$ for this analysis. The optimal value of α that maximizes the transmission distance is found to be the same in each case. The unit for the secure key rate r is bits per pulse.

arbitrarily, as there exists an optimal value that can maximize either the key rate or the total transmission distance. In Fig. 5, we plot the maximum transmission distance as a function of the coherent amplitude for various values of the secure key rate with an ideal detector, $\eta_d = 0$. We observe that there exists an optimal value, $\alpha \approx 0.5$, that maximizes the total transmission distance for any value of the secure key rate.

In Fig. 6, we plot the secure key rate as a function of the total transmission distance L for different values of η_d. We

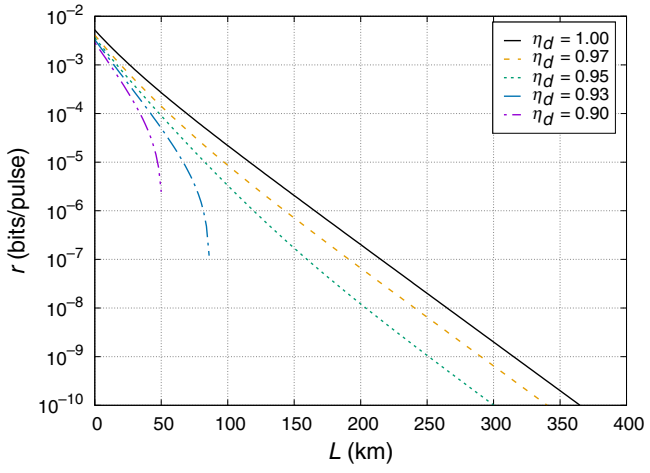

FIG. 6. Secure key rate as a function of total transmission distance L for different values of η_d in the optimal case, i.e., $\alpha = 0.5$. We assume detection efficiencies $\eta_h = 0.55$ for the homodyne detectors and $\eta_0 = 0.8$ for the ON-OFF detectors, and $p = \pi/2$.

choose $\eta_h = 0.55$, $\eta_0 = 0.8$, and $p = \pi/2$ to be as realistic as possible and simulate the results for a standard telecommunication fiber with $l = 0.2$ dB/km. Furthermore, the value of the coherent amplitude α is chosen to maximize the secure key rate over long transmission distances instead of entanglement. For our analysis we choose $\alpha = 0.5$ to optimize the total distance. It is also approximately the same value that optimizes the logarithmic negativity of an HE state when its CV part undergoes high photon loss. It is seen that under lower errors on Alice's and Bob's side ($\eta_d = 0.97$ and 0.95), a secure key rate can be achieved for transmission distances of around 300 km, indicating that the resultant entangled state is useful. However, the maximum achievable distance drastically falls off as η_d is increased up to 0.90.

IV. DISCUSSION AND CONCLUSION

We have shown that HE states between CV and DV systems provide a robust practical solution to the problem of achieving long-distance high-rate entanglement. Both requirements are fundamental for a number of applications. In this paper we have benchmarked the usefulness of the prepared entangled state using an EBQKD protocol, as it is both a fundamental application and a multipurpose test bed. In an EBQKD setup, our results indicate that HE states bring out the best of both CV and DV systems, resulting in a secure key rate of approximately 10^{-9} bits per pulse at a distance of 250 km with 5% detection inefficiency. This, in itself, represents a significant contribution. All this was achieved without the use of an ultralow-loss fiber (with channel loss $l = 0.16$ dB/km at 1550 nm [50]), which allowed an earlier study to achieve transmission distances greater than 400 km. With such a fiber, our approach would allow us to achieve approximately 10^{-10} bits per pulse at a distance of 300 km for $\eta_d = 0.95$.

In our analysis, it should be noted that, for of simplicity, we do not consider any thermal noise in the channels. However, one can qualitatively show that incorporating a practical value for such thermal noise will not significantly affect our results (see Appendix F for details).

We leave the detailed quantitative analysis in the presence of thermal noise for future work and acknowledge that it involves lengthy analytical calculations that may have an insignificant impact on our findings.

The feasibility of our protocol relies on the fact that HE states with small coherent amplitudes ($\alpha < 1$) can be generated in the laboratory by several nondeterministic techniques [34,35] and the generation rate is comparable to the rate of production of entangled photon pairs in parametric down-conversion setups. As an example, it is possible to prepare HE states where the CV and DV parts correspond

to the photon-number state and the coherent state, respectively, with fidelity of approximately 0.75 for $\alpha = 0.5$ [34]. While the rate of generation in the source is comparable to that of parametric down-conversion sources, losses during transmission are reduced, so the effective rate at the destination increases. The fidelity of the preparation could be a limiting factor. However, this can be mitigated by the use of other forms of HE states, most notably with the CV and DV modes corresponding to cat states and polarization, respectively, which offer exceptionally good fidelity of preparation as well as rate of generation [51–55]. We also note that a recent result indicates that it is also possible to deterministically generate HE states with high fidelity [56]

However, it should be noted that there will be effects from phase modulations and phase mismatch in a practical implementation of our scheme. Commercially available lasers, used in the generation of HE states, generally do not have well-defined phase stabilization while optical fibers, used for transmission, may introduce nonlinear effects on the signals. This causes additional concerns for phase locking and phase tracking to ensure successful interference at Charlie's end. Although such issues have been managed in the context of twin-field QKD [57], it remains unclear to us whether a similar architecture could be useful in our setup as well, and we leave it as an open avenue for future discussions.

Our results highlight the significance of HE states as a resource in high-rate remote entanglement generation, which plays a crucial role in enhancing many quantum information processing tasks, such as the quantum internet [58,59], quantum digital signature [60,61], and network steering [62]. We believe that our scheme has the potential to drive a new generation of experimental developments in quantum information technology.

ACKNOWLEDGMENTS

The authors thank Stefano Pirandola and Hua-Lei Yin for their comments on an earlier version of the manuscript. This work was supported by QuantERA grant SECRET, by AEI [63] (Project No. PCI2019-111885-2), by National Research Foundation of Korea grants funded by the Korean government (Grants No. NRF-2022M3K4A 1097117 and No. NRF-2023R1A2C1006115) via the Institute of Applied Physics at Seoul National University, and by Institute for Information and Communications Technology Planning and Evaluation (IITP) grants funded by the government of Korea (MSIT) (Grants No. IITP-2021-0-01059 and No. IITP-2023-2020-0-01606). A.C. is also supported by AEI [63] (Project No. PID2020-113738GB-I00). J.S. acknowledges support by the National Science and Technological Council of Taiwan through Grants No. NSTC 112-2628-M-006-007-MY4 and No. NSTC 112-2811-M-006-033-MY4.

APPENDIX A: GENERATION OF THE HYBRID ENTANGLED STATE

In this appendix, we outline a process, using a setup in line with the setup in Ref. [34], that can be used to experimentally generate an HE state of the form

$$|\psi\rangle_{ab} = \frac{1}{\sqrt{2}}\left(|0\rangle_a|\alpha\rangle_b + |1\rangle_a|-\alpha\rangle_b\right) \tag{A1}$$

between modes a and b, where $|0\rangle$ and $|1\rangle$ correspond to photon-number states and $|\alpha\rangle$ is the coherent state with coherent amplitude α.

$|n\rangle$ and $|\alpha\rangle$ correspond to, respectively, the energy eigenstate and the coherent state of a quantized electromagnetic field, where n is the number of photons in the state. It is possible to realize the energy eigenstates as a single-photon qubit by considering only the photon-number states corresponding to $|0\rangle$ and $|1\rangle$. This is our DV system, and the multiphoton coherent state is our CV system. The key idea of HE-state generation hinges on conditional photon addition and erasing the path information of photon addition. There are several ways of achieving photon addition. They include a model that uses single-photon sources and BSs and a model that uses a parametric down-converter (PDC) with a weak pump. Since the BS setup and the parametric down-converter are equivalent [64], here we use the BS model for photon addition. The following is a step-by-step description of the generation of the HE state in Fig. 1(b).

Step 1: A vacuum state $|0\rangle$ in mode a is mixed with a single-photon state $|1\rangle$ in mode c with the use of a BS (BS1) with transmittance T. Similarly, a coherent state $|\alpha\rangle$ in mode c is mixed with another single-photon state in mode d with the use of another BS (BS2) with transmittance T. The output states from each of these BSs are

$$\begin{aligned} |\psi\rangle_{ac}^{\mathrm{BS1}} &= \sqrt{1-T}\,|1\rangle_a|0\rangle_c + \sqrt{T}\,|0\rangle_a|1\rangle_c\,, \\ |\psi\rangle_{bd}^{\mathrm{BS2}} &= \sqrt{1-T}\hat{b}^\dagger|\alpha\rangle_b|0\rangle_d + \sqrt{T}\,|\alpha\rangle_b|1\rangle_d\,, \end{aligned} \tag{A2}$$

where $\hat{b}^\dagger$ is the creation operator acting on mode b and $|\psi\rangle_{ac}^{\mathrm{BS1}}$ is the output state from BS1, while $|\psi\rangle_{bd}^{\mathrm{BS2}}$ is the output state from BS2. The BS transmittance T can be fine-tuned according to experimental requirements to yield maximum probability for photon addition. Therefore, the four-mode state at the output of BS1 and BS2 is

$$\begin{aligned} |\psi\rangle_{ab,cd}^{\mathrm{BS1,2}} = \sqrt{T(1-T)}\Big(&|1\rangle_a|\alpha\rangle_b \otimes |0\rangle_c|1\rangle_d \\ &+ |0\rangle_a\hat{b}^\dagger|\alpha\rangle_b \otimes |1\rangle_c|0\rangle_d\Big) \\ &+ (1-T)\,|1\rangle_a\hat{b}^\dagger|\alpha\rangle_b \otimes |0\rangle_c|0\rangle_d \\ &+ T\,|0\rangle_a|\alpha\rangle_b \otimes |1\rangle_c|1\rangle_d\,. \end{aligned} \tag{A3}$$

Step 2: The outgoing single-photon modes [shown by dashed gray lines in Fig. 1(b)] from both BS1 and BS3 are mixed with each other with the use of a another BS (BS3), with transmittance τ. This leads to a four-mode state at the output of BS3 that can be written as

$$\begin{aligned}|\psi\rangle_{ab,cd}^{\mathrm{BS3}} = \sqrt{T(1-T)}\Big[|1\rangle_a|\alpha\rangle_b \otimes \Big(-\sqrt{1-\tau}\,|0\rangle_c|1\rangle_d + \sqrt{\tau}\,|1\rangle_c|0\rangle_d\Big) \\ + |0\rangle_a \hat{b}^\dagger|\alpha\rangle_b \otimes \Big(\sqrt{1-\tau}\,|1\rangle_c|0\rangle_d + \sqrt{\tau}\,|0\rangle_c|1\rangle_d\Big)\Big] \\ + (1-T)|1\rangle_a \hat{b}^\dagger|\alpha\rangle_b \otimes |0\rangle_c|0\rangle_d + T|0\rangle_a|\alpha\rangle_b \otimes \Big(\sqrt{1-\tau}\,|2\rangle_c|0\rangle_d + \sqrt{\tau}\,|0\rangle_c|2\rangle_d\Big). \end{aligned} \tag{A4}$$

Step 3: We now detect the output modes of BS3 via single-photon detectors D1 and D2. Since the total photon number at the output of BS3 is 1, this indicates that both detector D1 and detector D2 cannot click simultaneously. We postselect the state when only detector D1 clicks and discard the runs whenever detector D2 clicks. After postselection, the state between modes a and b is given as

$$\begin{aligned}|\psi\rangle_{ab}^{\mathrm{D1}} &= \langle 1|_c\langle 0|_d|\psi\rangle_{ab,cd}^{\mathrm{BS3}} \\ &= \sqrt{T(1-T)}\Big(\sqrt{\tau}\,|1\rangle_a|\alpha\rangle_b + \sqrt{1-\tau}\,|0\rangle_a\hat{b}^\dagger|\alpha\rangle_b\Big). \end{aligned} \tag{A5}$$

We can now use the fact that the n-photon-added coherent state is a good approximation to another coherent state with amplified amplitude, i.e., $\hat{b}^{\dagger n}/\sqrt{N}\,|\alpha\rangle \approx |g\alpha\rangle$ [34], where N is the corresponding normalization constant and $g \geq 1$ is the amplification factor. This leads to the result $\hat{b}^\dagger|\alpha\rangle_b \approx 1/\sqrt{1-\alpha^2}\,|g\alpha\rangle_b$, where g is properly chosen. Then, by setting $\tau = (1+\alpha^2)/(2+\alpha^2)$ and using the approximation, we get

$$|\psi\rangle_{ab}^{\mathrm{D1}} \approx \sqrt{\frac{T(1-T)}{2+\alpha^2}}\Big(|1\rangle_a|\alpha\rangle_b + |0\rangle_a|g\alpha\rangle_b\Big). \tag{A6}$$

Step 4: Next, we displace mode b by applying a displacement operator on this mode given by $D_b\left(-(\alpha+g\alpha)/2\right) = \exp\left[-(\alpha+g\alpha)/2(\hat{b}^\dagger - \hat{b})\right]$, where $\hat{b}$ is the annihilation operator. This leads to the final normalized HE state

$$|\psi\rangle_{ab} = \frac{1}{\sqrt{2}}\left(|0\rangle_a|\alpha_f\rangle_b + |1\rangle_a|-\alpha_f\rangle_b\right), \tag{A7}$$

where $\alpha_f = (g-1)\alpha/2$.

APPENDIX B: SHARED ENTANGLED STATE BETWEEN ALICE AND BOB

In this appendix, we calculate the state obtained after Charlie has performed the entanglement-swapping operation. We also calculate the states obtained after every step of the protocol starting from the initial resource of HE states. The steps of the protocol are detailed in the main text.

1. Initial states and channel transmission

We denote the two hybrid entangled states with Alice and Bob as

$$\begin{aligned}|\psi\rangle_{a_1a_2} &= \frac{1}{\sqrt{2}}\left(|0\rangle_{a_1}|\alpha\rangle_{a_2} + |1\rangle_{a_1}|-\alpha\rangle_{a_2}\right), \\ |\psi\rangle_{b_1b_2} &= \frac{1}{\sqrt{2}}\left(|0\rangle_{b_1}|\alpha\rangle_{b_2} + |1\rangle_{b_1}|-\alpha\rangle_{b_2}\right), \end{aligned} \tag{B1}$$

respectively. The initial four-mode resource state can be written as

$$\begin{aligned}|\psi\rangle_{\substack{a_1a_2\\b_1b_2}} &= |\psi\rangle_{a_1a_2}|\psi\rangle_{b_1b_2} \\ &= \frac{1}{2}\big(|00\rangle_{a_1b_1}|\alpha\rangle_{a_2}|\alpha\rangle_{b_2} + |11\rangle_{a_1b_1}|-\alpha\rangle_{a_2}|-\alpha\rangle_{b_2} \\ &\quad + |01\rangle_{a_1b_1}|\alpha\rangle_{a_2}|-\alpha\rangle_{b_2} + |10\rangle_{a_1b_1}|-\alpha\rangle_{a_2}|\alpha\rangle_{b_2}\big), \end{aligned} \tag{B2}$$

where $|ij\rangle_{a_1b_1} = |i\rangle_{a_1}|j\rangle_{b_1}$ for all $i,j \in \{0,1\}$.

Alice and Bob both send their multiphoton part (modes a_2 and b_2) to a third, distant party, Charlie, for mixing and subsequent measurements through a noisy/lossy channel with transmittance T. Such channels can be modeled in terms of an effective BS with transmittance T, where the input state is fed into one of the inputs of the BS, while the other input is initialized as a vacuum state. The action of a BS with transmittance T on the input modes is given by a unitary U_T^{ab} implementing the following transformation:

$$\begin{pmatrix}\hat{a}\\ \hat{b}\end{pmatrix} \to \begin{pmatrix}\hat{a}'\\ \hat{b}'\end{pmatrix} = \begin{pmatrix}\sqrt{T} & \sqrt{1-T}\\ -\sqrt{1-T} & \sqrt{T}\end{pmatrix}\begin{pmatrix}\hat{a}\\ \hat{b}\end{pmatrix}. \tag{B3}$$

$T = \frac{1}{2}$ corresponds to a balanced (50:50) BS. As a consequence, the action of the channel on a coherent state ($|\alpha\rangle$) in mode a is described as $U_T^{ab}|\alpha\rangle_a \otimes |0\rangle_b \to |\alpha\rangle_{a'} \otimes |0\rangle_{b'} = |\sqrt{T}\alpha\rangle_a \otimes |\sqrt{1-T}\alpha\rangle_b$, where U_T^{ab} is the corresponding BS unitary operation. Subsequently, the resultant state is obtained by our tracing over the ancillary mode b.

Similarly, the noisy transmission of modes a_2 and b_2 can be described by the use of two BSs with transmittance T, each in the paths of modes a_2 and b_2 with ancillary modes given by f_a and f_b, respectively. The resultant noisy/lossy state is obtained by our tracing over the ancillary modes (f_a and f_b). Therefore, the total input state for Charlie before mixing is given as

$$\begin{aligned}
|\psi\rangle_{\substack{a_1,b_1;a_2',b_2'\\ f_a',f_b'}} &= U_T^{(a_2,f_a)} \otimes U_T^{(b_2,f_b)} \, |\psi\rangle_{\substack{a_1a_2\\ b_1b_2}} \otimes |0\rangle_{f_a} |0\rangle_{f_b} \\
&= \frac{1}{2}\Big(|00\rangle_{a_1b_1} |\sqrt{1-T}\alpha\rangle_{f_a} |\sqrt{1-T}\alpha\rangle_{f_b} |\sqrt{T}\alpha\rangle_{a_2} |\sqrt{T}\alpha\rangle_{b_2} \\
&\quad + |11\rangle_{a_1b_1} |-\sqrt{1-T}\alpha\rangle_{f_a} |-\sqrt{1-T}\alpha\rangle_{f_b} |-\sqrt{T}\alpha\rangle_{a_2} |-\sqrt{T}\alpha\rangle_{b_2} \\
&\quad + |01\rangle_{a_1b_1} |\sqrt{1-T}\alpha\rangle_{f_a} |-\sqrt{1-T}\alpha\rangle_{f_b} |\sqrt{T}\alpha\rangle_{a_2} |-\sqrt{T}\alpha\rangle_{b_2} \\
&\quad + |10\rangle_{a_1b_1} |-\sqrt{1-T}\alpha\rangle_{f_a} |\sqrt{1-T}\alpha\rangle_{f_b} |-\sqrt{T}\alpha\rangle_{a_2} |\sqrt{T}\alpha\rangle_{b_2} \Big),
\end{aligned} \tag{B4}$$

where $U_T^{(a_2,f_a)}$ and $U_T^{(b_2,f_b)}$ are the BS unitary operations corresponding to the respective channels with transmittance T. Charlie now mixes the incoming multiphoton modes (a_2 and b_2) through a balanced BS (BS1), leading to the four-mode entangled state

$$\begin{aligned}
|\psi\rangle^{\mathrm{BS1}}_{\substack{a_1,b_1;a_2'',b_2''\\ f_a',f_b'}} &= U_{\mathrm{BS1}}^{(a_2,b_2)} \, |\psi\rangle_{\substack{a_1,b_1;a_2',b_2'\\ f_a',f_b'}} \\
&= \frac{1}{2}\Big(|00\rangle_{a_1b_1} |\sqrt{1-T}\alpha\rangle_{f_a} |\sqrt{1-T}\alpha\rangle_{f_b} |0\rangle_{b_2} |\sqrt{2T}\alpha\rangle_{a_2} \\
&\quad + |11\rangle_{a_1b_1} |-\sqrt{1-T}\alpha\rangle_{f_a} |-\sqrt{1-T}\alpha\rangle_{f_b} |0\rangle_{b_2'} |-\sqrt{2T}\alpha\rangle_{a_2} \\
&\quad + |01\rangle_{a_1b_1} |\sqrt{1-T}\alpha\rangle_{f_a} |-\sqrt{1-T}\alpha\rangle_{f_b} |\sqrt{2T}\alpha\rangle_{b_2} |0\rangle_{a_2} \\
&\quad + |10\rangle_{a_1b_1} |-\sqrt{1-T}\alpha\rangle_{f_a} |\sqrt{1-T}\alpha\rangle_{f_b} |-\sqrt{2T}\alpha\rangle_{b_2} |0\rangle_{a_2} \Big).
\end{aligned} \tag{B5}$$

It can be seen from Eq. (B5) that, in the total four-mode entangled state after mixing by Charlie, the vacuum-state contribution in mode a_2 appears with probability $1/2$. Our primary aim is to postselect the state (B5) in $|0\rangle_{a_2}$.

2. State after the ON-OFF measurement

The additional coherent state sent by Bob to Charlie $\left(|\sqrt{2}\alpha\rangle\right)$ becomes $|\sqrt{2T}\alpha\rangle$ as a result of transmission through the lossy channel. As described in Ref. [34], for this purpose Charlie first mixes the outgoing mode a_2 with this additional state $\left(|\sqrt{2T}\alpha\rangle\right)$ in mode c through the second balanced beam splitter (BS2). Consequently, the state after the mixing at BS2 is given by

$$\begin{aligned}
|\psi\rangle^{\mathrm{BS2}}_{\substack{a_1,b_1;b_2''\\ f_a',f_b'\\ a_2'',c'}} &= U_{\mathrm{BS1}}^{(a_2,c)} \, |\psi\rangle^{\mathrm{BS1}}_{\substack{a_1,b_1;a_2'',b_2''\\ f_a',f_b'}} \otimes |\sqrt{2T}\alpha\rangle_c \\
&= \frac{1}{2}\Big(|00\rangle_{a_1b_1} |\sqrt{1-T}\alpha\rangle_{f_a} |\sqrt{1-T}\alpha\rangle_{f_b} |0\rangle_{b_2} |2\sqrt{T}\alpha\rangle_{a_2} |0\rangle_c \\
&\quad + |11\rangle_{a_1b_1} |-\sqrt{1-T}\alpha\rangle_{f_a} |-\sqrt{1-T}\alpha\rangle_{f_b} |0\rangle_{b_2} |0\rangle_{a_2} |-2\sqrt{T}\alpha\rangle_c \\
&\quad + |01\rangle_{a_1b_1} |\sqrt{1-T}\alpha\rangle_{f_a} |-\sqrt{1-T}\alpha\rangle_{f_b} |\sqrt{2T}\alpha\rangle_{b_2} |\sqrt{T}\alpha\rangle_{a_2} |-\sqrt{T}\alpha\rangle_c \\
&\quad + |10\rangle_{a_1b_1} |-\sqrt{1-T}\alpha\rangle_{f_a} |\sqrt{1-T}\alpha\rangle_{f_b} |-\sqrt{2T}\alpha\rangle_{b_2} |\sqrt{T}\alpha\rangle_{a_2} |-\sqrt{T}\alpha\rangle_c \Big).
\end{aligned} \tag{B6}$$

As can be seen from Eq. (B6), if both detectors at the output of BS2 click, then the contribution can arise only from the respective part in Eq. (B6), i.e., from the part containing $|0\rangle_{a_2}$. Experimentally, this could be achieved unambiguously by

one performing the operation $\Pi_0 = (\mathbf{I} - |0\rangle\langle 0|) \otimes (\mathbf{I} - |0\rangle\langle 0|)$ on Eq. (B6) using two ON-OFF detectors at both output ports of BS2.

However, here we consider *nonideal* detectors with efficiency η_o ($0 \leq \eta_o \leq 1$). Similar to the case of transmission channels, this could be analyzed by considering two additional BS with transmittance η_o and two ancillary modes g_a and g_c for modes a_2 and c, respectively. Therefore, before the ON-OFF detectors, the total state is given by

$$
\begin{aligned}
|\psi\rangle^{\text{tot}}_{\substack{a_1,b_1;b_2'' \\ f_a' f_b' g_a' g_c' \\ a_2'''' c''}} &= U^{(a_2,g_a)}_{\eta_o} \otimes U^{(c,g_c)}_{\eta_o} |\psi\rangle^{\text{BS}_2}_{\substack{a_1,b_1;b_2'' \\ f_a' f_b' \\ a_2''' c'}} \otimes |0\rangle_{g_a} |0\rangle_{g_c} \\
&= \frac{1}{2}\Big[|00\rangle_{a_1b_1} |0\rangle_{b_2''} |\sqrt{1-T}\alpha\rangle_{f_a} |\sqrt{1-T}\alpha\rangle_{f_b} |2\sqrt{T(1-\eta_o)}\alpha\rangle_{g_a} |0\rangle_{g_c} |2\sqrt{T\eta_o}\alpha\rangle_{a_2} |0\rangle_c \\
&\quad + |11\rangle_{a_1b_1} |0\rangle_{b_2} |-\sqrt{1-T}\alpha\rangle_{f_a} |-\sqrt{1-T}\alpha\rangle_{f_b} |0\rangle_{g_a} |-2\sqrt{T(1-\eta_o)}\alpha\rangle_{g_c} |0\rangle_{a_2} |-2\sqrt{T\eta_o}\alpha\rangle_c \\
&\quad + \Big(|01\rangle_{a_1b_1} |\sqrt{2T}\alpha\rangle_{b_2} |\sqrt{1-T}\alpha\rangle_{f_a} |-\sqrt{1-T}\alpha\rangle_{f_b} + |10\rangle_{a_1b_1} |-\sqrt{2T}\alpha\rangle_{b_2} |-\sqrt{1-T}\alpha\rangle_{f_a} |\sqrt{1-T}\alpha\rangle_{f_b} \Big) \\
&\quad \times |\sqrt{T(1-\eta_o)}\alpha\rangle_{g_a} |-\sqrt{T(1-\eta_o)}\alpha\rangle_{g_c} |\sqrt{T\eta_0}\alpha\rangle_{a_2} |-\sqrt{T\eta_o}\alpha\rangle_c \Big] \\
&= \frac{1}{2}\Big[|00\rangle_{a_1b_1} |0\rangle_{b_2} |\sqrt{T'}\alpha\rangle_{f_a} |\sqrt{T'}\alpha\rangle_{f_b} |2\sqrt{T\eta_o'}\alpha\rangle_{g_a} |0\rangle_{g_c} |2\sqrt{T\eta_o}\alpha\rangle_{a_2} |0\rangle_c \\
&\quad + |11\rangle_{a_1b_1} |0\rangle_{b_2} |-\sqrt{T'}\alpha\rangle_{f_a} |-\sqrt{T'}\alpha\rangle_{f_b} |0\rangle_{g_a} |-2\sqrt{T\eta_o'}\alpha\rangle_{g_c} |0\rangle_{a_2} |-2\sqrt{T\eta_o}\alpha\rangle_c \\
&\quad + \Big(|01\rangle_{a_1b_1} |\sqrt{2T}\alpha\rangle_{b_2} |\sqrt{T'}\alpha\rangle_{f_a} |-\sqrt{T'}\alpha\rangle_{f_b} + |10\rangle_{a_1b_1} |-\sqrt{2T}\alpha\rangle_{b_2} |-\sqrt{T'}\alpha\rangle_{f_a} |\sqrt{T'}\alpha\rangle_{f_b} \Big) \\
&\quad \times |\sqrt{T\eta_o'}\alpha\rangle_{g_a} |-\sqrt{T\eta_o'}\alpha\rangle_{g_c} |\sqrt{T\eta_0}\alpha\rangle_{a_2} |-\sqrt{T\eta_o}\alpha\rangle_c \Big],
\end{aligned} \tag{B7}
$$

where $T' = 1 - T$ and $\eta_o' = 1 - \eta_o$.

Charlie is now supposed to make the measurement of $\Pi_0^{a_2,c} = (\mathbb{1} - |0\rangle\langle 0|)_{a_2} \otimes (\mathbb{1} - |0\rangle\langle 0|)_c$ on the state in Eq. (B7). After the measurement of these operators (Π_0), the total state collapses to $\rho^0_{a_1,b_1;b_2} = \underset{\substack{g_a,g_c \\ a_2,c}}{\text{tr}_{f_a,f_b}} \Big(|\psi_0\rangle\langle\psi_0| \Big)/N_0$, where $|\psi_0\rangle = \Pi_0^{a_2,c} |\psi\rangle^{\text{tot}}_{\substack{a_1,b_1;b_2'' \\ f_a' f_b' g_a' g_c' \\ a_2'''' c''}}$ and the normalization constants are $N_0 = \underset{f_a,f_b,g_a,g_c}{\text{tr}_{a_1,b_1,a_2,b_2,c}} \Big(|\psi_0\rangle\langle\psi_0| \Big)$. It must be noted that the state $\rho^0_{a_1,b_1;b_2}$ is obtained with probability $P_0 = \underset{b_2}{\text{tr}_{a_1,b_1}} \Big(\rho^0_{a_1,b_1;b_2} \Big)$.

Let us fist look at the result

$$
\begin{aligned}
\Pi_0^{a_2,c} |\alpha\rangle_{a_2} |\beta\rangle_c &= \Big(\mathbb{1}_{a_2} \otimes \mathbb{1}_c - |0\rangle_{a_2}\langle 0| \otimes \mathbb{1}_c - \mathbb{1}_{a_2} \otimes |0\rangle_c\langle 0| + |0\rangle_{a_2}\langle 0| \otimes |0\rangle_c\langle 0| \Big) |\alpha\rangle_{a_2} |\beta\rangle_c \\
&= |\alpha\rangle_{a_2} |\beta\rangle_c - e^{-\alpha^2/2} |0\rangle_{a_2} |\beta\rangle_c - e^{-\beta^2/2} |\alpha\rangle_{a_2} |0\rangle_c + e^{-(\alpha^2+\beta^2)/2} |0\rangle_{a_2} |0\rangle_c ,
\end{aligned} \tag{B8}
$$

leading to

$$
\begin{aligned}
\Pi_0^{a_2,c} |\alpha\rangle_{a_2} |0\rangle_c &= \Pi_0^{a_2,c} |0\rangle_{a_2} |\alpha\rangle_c = 0, \\
\Pi_0^{a_2,c} |\alpha\rangle_{a_2} |-\alpha\rangle_c &= |\alpha\rangle_{a_2} |-\alpha\rangle_c - e^{-\alpha^2/2} |0\rangle_{a_2} |-\alpha\rangle_c - e^{-\alpha^2/2} |\alpha\rangle_{a_2} |0\rangle_c + e^{-\alpha^2} |0\rangle_{a_2} |0\rangle_c .
\end{aligned} \tag{B9}
$$

Using the results of Eq. (B9) in Eq. (B7), we obtain

$$
\begin{aligned}
|\psi_0\rangle &= \Pi_0^{a_2,c} |\psi\rangle^{\text{tot}}_{\substack{a_1,b_1;b_2'' \\ f_a' f_b' g_a' g_c' \\ a_2'''' c''}} \\
&= \frac{1}{2}\Big[|00\rangle_{a_1b_1} |0\rangle_{b_2} |\sqrt{T'}\alpha\rangle_{f_a} |\sqrt{T'}\alpha\rangle_{f_b} \otimes |2\sqrt{T\eta_o'}\alpha\rangle_{g_a} |0\rangle_{g_c} \times 0 \\
&\quad + |11\rangle_{a_1b_1} |0\rangle_{b_2} |-\sqrt{T'}\alpha\rangle_{f_a} |-\sqrt{T'}\alpha\rangle_{f_b} \otimes |0\rangle_{g_a} |-2\sqrt{T\eta_o'}\alpha\rangle_{g_c} \times 0
\end{aligned}
$$

$$
\begin{aligned}
&+\left(|01\rangle_{a_1b_1}|\sqrt{2T}\alpha\rangle_{b_2}|\sqrt{T'}\alpha\rangle_{f_a}|-\sqrt{T'}\alpha\rangle_{f_b}+|10\rangle_{a_1b_1}|-\sqrt{2T}\alpha\rangle_{b_2}|-\sqrt{T'}\alpha\rangle_{f_a}|\sqrt{T'}\alpha\rangle_{f_b}\right)\otimes|\sqrt{T\eta_o'}\alpha\rangle_{g_a}|-\sqrt{T\eta_o'}\alpha\rangle_{g_c}\\
&\otimes\left(|\sqrt{\eta_oT}\alpha\rangle_{a_2}|-\sqrt{\eta_oT}\alpha\rangle_c-e^{-\eta_oT\alpha^2/2}|0\rangle_{a_2}|-\sqrt{\eta_oT}\alpha\rangle_c-e^{-\eta_oT\alpha^2/2}|\sqrt{\eta_oT}\alpha\rangle_{a_2}|0\rangle_c+e^{-\eta_oT\alpha^2}|0\rangle_{a_2}|0\rangle_c\right)\Big]\\
&=\frac{1}{2}\left(|01\rangle_{a_1b_1}|\sqrt{2T}\alpha\rangle_{b_2}|\sqrt{T'}\alpha\rangle_{f_a}|-\sqrt{T'}\alpha\rangle_{f_b}+|10\rangle_{a_1b_1}|-\sqrt{2T}\alpha\rangle_{b_2}|-\sqrt{T'}\alpha\rangle_{f_a}|\sqrt{T'}\alpha\rangle_{f_b}\right)\\
&\otimes|\sqrt{T\eta_o'}\alpha\rangle_{g_a}|-\sqrt{T\eta_o'}\alpha\rangle_{g_c}\otimes|\Psi\rangle_{a_2c},
\end{aligned}
\tag{B10}
$$

where

$$
|\Psi\rangle_{a_2c}=|\sqrt{\eta_oT}\alpha\rangle_{a_2}|-\sqrt{\eta_oT}\alpha\rangle_c-e^{-\eta_oT\alpha^2/2}|0\rangle_{a_2}|-\sqrt{\eta_oT}\alpha\rangle_c-e^{-\eta_oT\alpha^2/2}|\sqrt{\eta_oT}\alpha\rangle_{a_2}|0\rangle_c+e^{-\eta_oT\alpha^2}|0\rangle_{a_2}|0\rangle_c. \tag{B11}
$$

It can be further shown that

$$
\begin{aligned}
\mathrm{tr}\Big(|\Psi\rangle_{a_2c}\langle\Psi|\Big)&=\mathrm{tr}\Big[\Big(\langle\sqrt{\eta_oT}\alpha|\,|\sqrt{\eta_oT}\alpha\rangle\langle-\sqrt{\eta_oT}\alpha|\,|-\sqrt{\eta_oT}\alpha\rangle+e^{-\eta_oT\alpha^2}\langle0|\,|0\rangle\langle-\sqrt{\eta_oT}\alpha|\,|-\sqrt{\eta_oT}\alpha\rangle\\
&\quad+e^{-\eta_oT\alpha^2}\langle\sqrt{\eta_oT}\alpha|\,|\sqrt{\eta_oT}\alpha\rangle\langle0|\,|0\rangle+e^{-2\eta_oT\alpha^2}\langle0|\,|0\rangle\langle0|\,|0\rangle\Big)\\
&\quad+2\Big(-e^{-\eta_oT\alpha^2/2}\langle0|\,|\sqrt{\eta_oT}\alpha\rangle\langle-\sqrt{\eta_oT}\alpha|\,|-\sqrt{\eta_oT}\alpha\rangle-e^{-\eta_oT\alpha^2/2}\langle\sqrt{\eta_oT}\alpha|\,|\sqrt{\eta_oT}\alpha\rangle\langle0|\,|-\sqrt{\eta_oT}\alpha\rangle\\
&\quad+e^{-\eta_oT\alpha^2}\langle0|\,|\sqrt{\eta_oT}\alpha\rangle\langle0|\,|-\sqrt{\eta_oT}\alpha\rangle\Big)+2\Big(e^{-\eta_oT\alpha^2}\langle\sqrt{\eta_oT}\alpha|\,|0\rangle\langle0|\,|-\sqrt{\eta_oT}\alpha\rangle\\
&\quad-e^{-3\eta_oT\alpha^2/2}\langle0|\,|0\rangle\langle0|\,|-\sqrt{\eta_oT}\alpha\rangle\Big)-2e^{-3\eta_oT\alpha^2/2}\langle0|\,|\sqrt{\eta_oT}\alpha\rangle\langle0|\,|0\rangle\Big]\\
&=\left(1+e^{-\eta_oT\alpha^2}+e^{-\eta_oT\alpha^2}+e^{-2\eta_oT\alpha^2}\right)+2\left(-e^{-\eta_oT\alpha^2}-e^{-\eta_oT\alpha^2}+e^{-2\eta_oT\alpha^2}\right)\\
&\quad+2\left(e^{-2\eta_oT\alpha^2}-e^{-2\eta_oT\alpha^2}\right)-2e^{-2\eta_oT\alpha^2}\\
&=1-2e^{-\eta_oT\alpha^2}+e^{-2\eta_oT\alpha^2}=\left(1-e^{-\eta_oT\alpha^2}\right)^2.
\end{aligned}
\tag{B12}
$$

Hence,

$$
\begin{aligned}
\mathrm{tr}_{\substack{f_a,f_b\\g_a,g_c\\a_2,c}}\Big(|\psi_0\rangle\langle\psi_0|\Big)&=\frac{\left(1-e^{-\eta_oT\alpha^2}\right)^2}{4}\mathrm{tr}_{f_a,f_b}\Big[\Big(|01\rangle_{a_1b_1}\langle01|\otimes|\sqrt{2T}\alpha\rangle_{b_2}\langle\sqrt{2T}\alpha|\otimes|\sqrt{T'}\alpha\rangle_{f_a}\langle\sqrt{T'}\alpha|\otimes|-\sqrt{T'}\alpha\rangle_{f_b}\langle-\sqrt{T'}\alpha|\\
&\quad+|10\rangle_{a_1b_1}\langle10|\otimes|-\sqrt{2T}\alpha\rangle_{b_2}\langle-\sqrt{2T}\alpha|\otimes|-\sqrt{T'}\alpha\rangle_{f_a}\langle-\sqrt{T'}\alpha|\otimes|\sqrt{T'}\alpha\rangle_{f_b}\langle\sqrt{T'}\alpha|\\
&\quad+|01\rangle_{a_1b_1}\langle10|\otimes|\sqrt{2T}\alpha\rangle_{b_2}\langle-\sqrt{2T}\alpha|\otimes|\sqrt{T'}\alpha\rangle_{f_a}\langle-\sqrt{T'}\alpha|\otimes|-\sqrt{T'}\alpha\rangle_{f_b}\langle\sqrt{T'}\alpha|\\
&\quad+|10\rangle_{a_1b_1}\langle01|\otimes|-\sqrt{2T}\alpha\rangle_{b_2}\langle\sqrt{2T}\alpha|\otimes|-\sqrt{T'}\alpha\rangle_{f_a}\langle\sqrt{T'}\alpha|\otimes|\sqrt{T'}\alpha\rangle_{f_b}\langle-\sqrt{T'}\alpha|\Big)\Big]\\
&\quad\times\mathrm{tr}_{g_a,g_c}\Big[|\sqrt{T\eta_o'}\alpha\rangle_{g_a}\langle\sqrt{T\eta_o'}\alpha|\otimes|-\sqrt{T\eta_o'}\alpha\rangle_{g_c}\langle-\sqrt{T\eta_o'}\alpha|\Big]\\
&=\frac{\left(1-e^{-\eta_oT\alpha^2}\right)^2}{4}\Big[|01\rangle_{a_1b_1}\langle01|\otimes|\sqrt{2T}\alpha\rangle_{b_2}\langle\sqrt{2T}\alpha|+|10\rangle_{a_1b_1}\langle10|\otimes|-\sqrt{2T}\alpha\rangle_{b_2}\langle-\sqrt{2T}\alpha|\\
&\quad+\left(|01\rangle_{a_1b_1}\langle10|\otimes|\sqrt{2T}\alpha\rangle_{b_2}\langle-\sqrt{2T}\alpha|+|10\rangle_{a_1b_1}\langle01|\otimes|-\sqrt{2T}\alpha\rangle_{b_2}\langle\sqrt{2T}\alpha|\right)e^{-4(1-T)\alpha^2}\Big],
\end{aligned}
\tag{B13}
$$

where $\mathrm{tr}\Big(|\alpha\rangle\langle-\alpha|\Big) = e^{-2\alpha^2}$. The corresponding probability and normalization constant are given as

$$P_0 = N_0 = \mathrm{tr}_{\substack{a_1,b_1\\b_2}}\left[\mathrm{tr}_{\substack{f_a,f_b\\g_a,g_c\\a_2,c}}\Big(|\psi_0\rangle\langle\psi_0|\Big)\right] = \frac{\left(1-e^{-\eta_o T\alpha^2}\right)^2}{2}. \tag{B14}$$

This leads to the normalized state

$$\begin{aligned}\rho^0_{a_1,b_1,b_2} &= \frac{1}{N_0}\mathrm{tr}_{\substack{f_a,f_b\\g_a,g_c\\a_2,c}}\Big(|\psi_0\rangle\langle\psi_0|\Big)\\ &= \frac{1}{2}\Big[|01\rangle_{a_1b_1}\langle 01|\otimes|\sqrt{2T}\alpha\rangle_{b_2}\langle\sqrt{2T}\alpha| + |10\rangle_{a_1b_1}\langle 10|\otimes|-\sqrt{2T}\alpha\rangle_{b_2}\langle-\sqrt{2T}\alpha|\\ &\quad+\Big(|01\rangle_{a_1b_1}\langle 10|\otimes|\sqrt{2T}\alpha\rangle_{b_2}\langle-\sqrt{2T}\alpha|\\ &\quad+|10\rangle_{a_1b_1}\langle 01|\otimes|-\sqrt{2T}\alpha\rangle_{b_2}\langle\sqrt{2T}\alpha|\Big)e^{-4(1-T)\alpha^2}\Big].\end{aligned} \tag{B15}$$

3. Final state obtained after the homodyne measurement

Charlie now performs the homodyne measurement along the quadrature X_θ on mode b_2. Here we also consider that the homodyne instruments are not perfect. Rather the efficiency of the homodyne detector is given by η_h. Similarly to the earlier cases, here also the imperfect homodyne detector can be modeled as a passive beam splitter with transmittance η_h. Now the action of the imperfect homodyne measurement along quadrature X_θ will lead to the resultant unnormalized state $\rho^{\mathrm{hom},0}_{\mathrm{un}} = \langle X_\theta|_{b_2}\,\mathrm{tr}_{h_b}\left[\left(U^{h_b,b_2}_{\eta_h}\right)\rho^0_{a_1,b_1;b_2}\otimes|0\rangle_{h_b}\langle 0|\left(U^{h_b,b_2}_{\eta_h}\right)^\dagger\right]|X_\theta\rangle_{b_2}$ with normalization $N^{\mathrm{hom}}_0 = \mathrm{tr}_{a_1,b_1}\left(\rho^{\mathrm{hom},0}_{\mathrm{un}}\right)$, where X_θ in a mode a is defined as $X_\theta = (ae^{i\theta} + a^\dagger e^{i\theta})/2$ and with the eigenvalue equation as X_θ defined as $X_\theta|X_\theta\rangle = x_\theta|X_\theta\rangle$.

Thus, after the homodyne measurement by Charlie, the residual normalized state between Alice and Bob will be given by

$$\rho_{a_1,b_1} = \frac{\rho^{\mathrm{hom},0}_{\mathrm{un}}}{N^{\mathrm{hom}}_0}. \tag{B16}$$

In this work we consider the measurement of the quadrature operator for the choice of $\theta = \pi/2$, i.e., we consider the *momentumlike* quadrature operator P. Now the measurement of P for a coherent state $|\alpha\rangle$ is $\langle P|\alpha\rangle = (1/\pi^{1/4})e^{-p^2/2}e^{-\alpha^2-i\sqrt{2}\alpha p}$. Now

$$\begin{aligned}&\mathrm{tr}_{h_b}\left[\left(U^{h_b,b_2}_{\eta_h}\right)\rho^0_{a_1,b_1;b_2}\otimes|0\rangle_{h_b}\langle 0|\left(U^{h_b,b_2}_{\eta_h}\right)^\dagger\right]\\ &= \frac{1}{2}\mathrm{tr}_{h_b}\left\{\left(U^{h_b,b_2}_{\eta_h}\right)\Big[|01\rangle_{a_1b_1}\langle 01|\otimes|\sqrt{2T}\alpha\rangle_{b_2}\langle\sqrt{2T}\alpha| + |10\rangle_{a_1b_1}\langle 10|\otimes|-\sqrt{2T}\alpha\rangle_{b_2}\langle-\sqrt{2T}\alpha|\\ &\quad+\Big(|01\rangle_{a_1b_1}\langle 10|\otimes|\sqrt{2T}\alpha\rangle_{b_2}\langle-\sqrt{2T}\alpha| + |10\rangle_{a_1b_1}\langle 01|\otimes|-\sqrt{2T}\alpha\rangle_{b_2}\langle\sqrt{2T}\alpha|\Big)e^{-4(1-T)\alpha^2}\Big]\otimes|0\rangle_{h_b}\langle 0|\left(U^{h_b,b_2}_{\eta_h}\right)^\dagger\right\}\\ &= \frac{1}{2}\mathrm{tr}_{h_b}\Big[|01\rangle_{a_1b_1}\langle 01|\otimes|\sqrt{2T\eta_h}\alpha\rangle_{b_2}\langle\sqrt{2T\eta_h}\alpha|\otimes|\sqrt{2T\eta'_h}\alpha\rangle_{h_b}\langle\sqrt{2T\eta'_h}\alpha|\\ &\quad+|10\rangle_{a_1b_1}\langle 10|\otimes|-\sqrt{2T\eta_h}\alpha\rangle_{b_2}\langle-\sqrt{2T\eta_h}\alpha|\otimes|-\sqrt{2T\eta'_h}\alpha\rangle_{h_b}\langle-\sqrt{2T\eta'_h}\alpha|\\ &\quad+\Big(|01\rangle_{a_1b_1}\langle 10|\otimes|\sqrt{2T\eta_h}\alpha\rangle_{b_2}\langle-\sqrt{2T\eta_h}\alpha|\otimes|\sqrt{2T\eta'_h}\alpha\rangle_{h_b}\langle-\sqrt{2T\eta'_h}\alpha|\\ &\quad+|10\rangle_{a_1b_1}\langle 01|\otimes|-\sqrt{2T\eta_h}\alpha\rangle_{b_2}\langle\sqrt{2T\eta_h}\alpha|\otimes|-\sqrt{2T\eta'_h}\alpha\rangle_{h_b}\langle\sqrt{2T\eta'_h}\alpha|\Big)e^{-4(1-T)\alpha^2}\Big]\end{aligned}$$

$$
\begin{aligned}
&= \frac{1}{2}\Big[|01\rangle_{a_1b_1}\langle 01| \otimes |\sqrt{2T\eta_h}\alpha\rangle_{b_2}\langle\sqrt{2T\eta_h}\alpha| + |10\rangle_{a_1b_1}\langle 10| \otimes |-\sqrt{2T\eta_h}\alpha\rangle_{b_2}\langle-\sqrt{2T\eta_h}\alpha| \\
&\quad + \left(|01\rangle_{a_1b_1}\langle 10| \otimes |\sqrt{2T\eta_h}\alpha\rangle_{b_2}\langle-\sqrt{2T\eta_h}\alpha| + |10\rangle_{a_1b_1}\langle 01| \otimes |-\sqrt{2T\eta_h}\alpha\rangle_{b_2}\langle\sqrt{2T\eta_h}\alpha|\right) e^{-4T(1-\eta_h')\alpha^2} e^{-4(1-T)\alpha^2}\Big] \\
&= \frac{1}{2}\Big[|01\rangle_{a_1b_1}\langle 01| \otimes |\sqrt{2T\eta_h}\alpha\rangle_{b_2}\langle\sqrt{2T\eta_h}\alpha| + |10\rangle_{a_1b_1}\langle 10| \otimes |-\sqrt{2T\eta_h}\alpha\rangle_{b_2}\langle-\sqrt{2T\eta_h}\alpha| \\
&\quad + \left(|01\rangle_{a_1b_1}\langle 10| \otimes |\sqrt{2T\eta_h}\alpha\rangle_{b_2}\langle-\sqrt{2T\eta_h}\alpha| + |10\rangle_{a_1b_1}\langle 01| \otimes |-\sqrt{2T\eta_h}\alpha\rangle_{b_2}\langle\sqrt{2T\eta_h}\alpha|\right) e^{-4(1-T\eta_h)\alpha^2}\Big],
\end{aligned} \tag{B17}
$$

which leads to

$$
\begin{aligned}
\rho_{\rm un}^{\rm hom,0} &= \langle P|_{b_2}\,{\rm tr}_{h_b}\left[\left(U_{\eta_h}^{h_b,b_2}\right)\rho^0_{a_1,b_1;b_2}\otimes|0\rangle_{h_b}\langle 0|\left(U_{\eta_h}^{h_b,b_2}\right)^\dagger\right]|P\rangle_{b_2} \\
&= \frac{1}{2}\langle P|_{b_2}\Big[|01\rangle_{a_1b_1}\langle 01| \otimes |\sqrt{2T\eta_h}\alpha\rangle_{b_2}\langle\sqrt{2T\eta_h}\alpha| + |10\rangle_{a_1b_1}\langle 10| \otimes |-\sqrt{2T\eta_h}\alpha\rangle_{b_2}\langle-\sqrt{2T\eta_h}\alpha| \\
&\quad + \left(|01\rangle_{a_1b_1}\langle 10| \otimes |\sqrt{2T\eta_h}\alpha\rangle_{b_2}\langle-\sqrt{2T\eta_h}\alpha| + |10\rangle_{a_1b_1}\langle 01| \otimes |-\sqrt{2T\eta_h}\alpha\rangle_{b_2}\langle\sqrt{2T\eta_h}\alpha|\right) e^{-4(1-T\eta_h)\alpha^2}\Big]|P\rangle_{b_2} \\
&= \frac{e^{-p^2}}{2\sqrt{\pi}}\Big[|01\rangle_{a_1b_1}\langle 01|\, e^{-4T\eta_h\alpha^2} + |10\rangle_{a_1b_1}\langle 10|\, e^{-4T\eta_h\alpha^2} \\
&\quad + \left(|01\rangle_{a_1b_1}\langle 10|\, e^{-4T\eta_h\alpha^2-4i\sqrt{T\eta_h}\alpha p} + |10\rangle_{a_1b_1}\langle 01|\, e^{-4T\eta_h\alpha^2+4i\sqrt{T\eta_h}\alpha p}\right) e^{-4(1-T\eta_h)\alpha^2}\Big] \\
&= \frac{e^{-p^2}e^{-4T\eta_h\alpha^2}}{2\sqrt{\pi}}\Big[|01\rangle_{a_1b_1}\langle 01| + |10\rangle_{a_1b_1}\langle 10| + \left(|01\rangle_{a_1b_1}\langle 10|\, e^{-4i\sqrt{T\eta_h}\alpha p} + |10\rangle_{a_1b_1}\langle 01|\, e^{4i\sqrt{T\eta_h}\alpha p}\right) e^{-4(1-T\eta_h)\alpha^2}\Big],
\end{aligned} \tag{B18}
$$

with $N_0^{\rm hom} = {\rm tr}_{a_1,b_1}\left(\rho_{\rm un}^{\rm hom,0}\right) = e^{-p^2}e^{-4T\eta_h\alpha^2}/\sqrt{\pi}$.

Therefore,

$$
\begin{aligned}
\rho_{a_1,b_1} &= \frac{\rho_{\rm un}^{\rm hom,0}}{N_0^{\rm hom}} \\
&= \frac{1}{2}\Big[|01\rangle_{a_1b_1}\langle 01| + |10\rangle_{a_1b_1}\langle 10| + \Big(|01\rangle_{a_1b_1}\langle 10|\, e^{-4i\sqrt{T\eta_h}\alpha p} \\
&\quad + |10\rangle_{a_1b_1}\langle 01|\, e^{4i\sqrt{T\eta_h}\alpha p}\Big) e^{-4(1-T\eta_h)\alpha^2}\Big] \\
&= \frac{1}{2}\left[|01\rangle_{a_1b_1}\langle 01| + |10\rangle_{a_1b_1}\langle 10| + h\left(g\,|01\rangle_{a_1b_1}\langle 10| + g^*\,|10\rangle_{a_1b_1}\langle 01|\right)\right],
\end{aligned} \tag{B19}
$$

where $h = e^{-4(1-T\eta_h)\alpha^2}$ and $g = e^{-4i\sqrt{T\eta_h}\alpha p}$. The probability of obtaining this final state is given by $P_0 = \left(1 - e^{-\eta_o T\alpha^2}\right)^2/2$ [Eq. (B14)].

APPENDIX C: LOGARITHMIC NEGATIVITY OF HYBRID ENTANGLED STATES UNDERGOING PHOTON LOSS

In our protocol we use the CV part of the HE state for transmission via a lossy quantum channel. It can be shown that under photon losses in the CV part, an HE state can still retain correlations for a particular value of α.

We analyze the amount of correlations that an HE state retains after its CV system is transmitted via a lossy quantum channel. Upon transmission, the CV part undergoes photon loss that is directly dependent on the value of α chosen. We show that the correlations in an HE state after its CV part has undergone transmission loss are a nonmonotonic function of its coherent amplitude. Specifically, we evaluate the logarithmic negativity [65,66] of the initial HE state as a function of transmission loss. We find that for $\alpha \approx 0.5$, the HE state is highly robust regarding noise.

Let us consider the HE state

$$|\psi\rangle_{ab} = \frac{1}{\sqrt{2}}\Big(|0\rangle_a |\alpha\rangle_b + |1\rangle_a |-\alpha\rangle_b \Big). \tag{C1}$$

Suppose that mode b undergoes photon loss. The process of photon loss can be equivalently modeled as passage through a beam splitter with reflectivity R ($0 \leq R \leq 1$), while the other input to the beam splitter is taken to be a vacuum. In such a case, the beam-splitter matrix is

$$\begin{pmatrix} \sqrt{1-R} & \sqrt{R} \\ -\sqrt{R} & \sqrt{1-R} \end{pmatrix},$$

where $R = 0$ and $R = 1$ stand for zero photon loss and complete photon loss, respectively. Let us consider that mode b passes through such a beam splitter, while the other input is at $|0\rangle$ in mode c. As a consequence, the total state after passage through the beam splitter becomes

$$|\psi\rangle_{ab} \otimes |0\rangle_c \xrightarrow{\text{BS}} \frac{1}{\sqrt{2}} \left(|0\rangle_a |\sqrt{1-R}\alpha\rangle_b |\sqrt{R}\alpha\rangle_c + |1\rangle_a |-\sqrt{1-R}\alpha\rangle_b |-\sqrt{R}\alpha\rangle_c \right). \tag{C2}$$

Subsequently, the two-mode state in modes a and b after photon loss is obtained by our tracing over the ancillary mode c as

$$\begin{aligned}
\rho_{ab}^{\text{loss}} &= \text{tr}_c \Big[\frac{1}{2} \Big(|0, \sqrt{1-R}\alpha\rangle_{ab} \langle 0, \sqrt{1-R}\alpha| \otimes |\sqrt{R}\alpha\rangle_c \langle \sqrt{R}\alpha| + |1, -\sqrt{1-R}\alpha\rangle_{ab} \langle 1, -\sqrt{1-R}\alpha| \otimes |-\sqrt{R}\alpha\rangle_c \langle -\sqrt{R}\alpha| \\
&\quad + |0, \sqrt{1-R}\alpha\rangle_{ab} \langle 1, -\sqrt{1-R}\alpha| \otimes |\sqrt{R}\alpha\rangle_c \langle -\sqrt{R}\alpha| + |1, -\sqrt{1-R}\alpha\rangle_{ab} \langle 0, \sqrt{1-R}\alpha| \otimes |-\sqrt{R}\alpha\rangle_c \langle \sqrt{R}\alpha| \Big) \Big] \\
&= \frac{1}{2} \Big(|0, \sqrt{1-R}\alpha\rangle_{ab} \langle 0, \sqrt{1-R}\alpha| + |1, -\sqrt{1-R}\alpha\rangle_{ab} \langle 1, -\sqrt{1-R}\alpha| + e^{-2R\alpha^2} |0, \sqrt{1-R}\alpha\rangle_{ab} \langle 1, -\sqrt{1-R}\alpha| \\
&\quad + e^{-2R\alpha^2} |1, -\sqrt{1-R}\alpha\rangle_{ab} \langle 0, \sqrt{1-R}\alpha| \Big) \\
&= \frac{1}{2} \Big[|0\rangle_a \langle 0| \otimes |\sqrt{1-R}\alpha\rangle_b \langle \sqrt{1-R}\alpha| + |1\rangle_a \langle 1| \otimes |-\sqrt{1-R}\alpha\rangle_b \langle -\sqrt{1-R}\alpha| \\
&\quad + e^{-2R\alpha^2} \Big(|0\rangle_a \langle 1| \otimes |\sqrt{1-R}\alpha\rangle_b \langle -\sqrt{1-R}\alpha| + |1\rangle_a \langle 0| \otimes |-\sqrt{1-R}\alpha\rangle_b \langle \sqrt{1-R}\alpha| \Big) \Big].
\end{aligned} \tag{C3}$$

To evaluate the entanglement content in this state, we use logarithmic negativity as a measure of entanglement. For a bipartite state ρ_{ab}^{loss} it is defined as $E_N\left(\rho_{ab}^{\text{loss}}\right) = \log_2 \left|\left| \left(\rho_{ab}^{\text{loss}}\right)^{\text{PT}} \right|\right|_1$, where $||.||_1$ is the trace norm and PT stands for partial transpose over mode a or mode b. We evaluate the logarithmic negativity for the state after photon loss in Eq. (C3) numerically, and it is shown in the main text.

APPENDIX D: LOGARITHMIC NEGATIVITY OF THE SHARED ENTANGLED STATES

To evaluate the entanglement content in this state, we use logarithmic negativity as a measure of entanglement. For a bipartite state $\rho_{a_1b_1}$, it is defined as $E_N\left(\rho_{a_1b_1}\right) = \log_2 \left|\left| \rho_{a_1b_1}^{\text{PT}} \right|\right|_1$, where $||.||_1$ is the trace norm and PT stands for partial transpose over mode a_1 or or mode b_1. Here we evaluate the logarithmic negativity for the shared entangled state between Alice and Bob (B19) under partial transposition over mode b_1. The resultant state after the partial transpose is written as

$$\begin{aligned}
\rho_{a_1,b_1}^{\text{PT}} = \frac{1}{2} \big[&|01\rangle_{a_1b_1} \langle 01| + |10\rangle_{a_1b_1} \langle 10| \\
&+ h \left(g\, |00\rangle_{a_1b_1} \langle 11| + g^*\, |11\rangle_{a_1b_1} \langle 00| \right) \big],
\end{aligned} \tag{D1}$$

where $h = e^{-4(1-T\eta_h)\alpha^2}$ and $g = e^{-4i\sqrt{T\eta_h}\alpha p}$. This leads to the eigenvalues of $\rho_{a_1,b_1}^{\text{PT}}$ as $\lambda_1 = \lambda_2 = \frac{1}{2}$, $\lambda_3 = h/2$, and $\lambda_4 = -h/2$. As a consequence, the logarithmic negativity of $\rho_{a_1b_1}$ is given as

$$E_N\left(\rho_{a_1b_1}\right) = \log_2 \left(\sum_{k=1}^{4} |\lambda_k| \right) = \log_2 (1+h). \tag{D2}$$

However, it should be noted that the final state, $\rho_{a_1b_1}$, is produced only with probability P_0. Consequently, the entanglement between the parties is effectively given as $E_n\left(\rho_{a_1b_1}\right) = P_0 \log_2(1+h)$. The reason for multiplication with the probability P_0 is because it determines the rate of generation of the resultant entangled state. As an example, consider $\alpha = 0$. The HE state (A1) is effectively a separable state and therefore cannot yield any correlations after swapping. This behavior is captured by the fact that the final entangled state is produced with probability 0. However, if we only look at the state $\rho_{a_1b_1}$, we find that it is maximally entangled with logarithmic negativity equal to 1. Therefore, it is necessary to include the rate of production in the analysis of entanglement of the final state.

APPENDIX E: ANALYSIS OF THE SECURE KEY RATE

In this appendix, we first provide a description of the optimal strategy of an eavesdropper, Eve—namely, an entangling cloner attack. Then we provide a detailed analysis of the secure key rate under this strategy by Eve.

1. Evaluation of the secured key rate

To evaluate the secure key rate, we assume the existence of an eavesdropper, Eve, with system E. We assume that Eve can potentially collaborate with the untrusted party, Charlie, while also having access to the two quantum channels that are used to transmit the CV systems. We also consider that Eve can perform an entangling cloner attack on each of the quantum channels [48,67,68]. However, the most-general attack strategy with Eve is a two-mode correlated attack (one mode for each quantum channel). Since, Alice and Bob use a CV system for transmission purposes, the aforementioned attacks have been shown to be the optimal choices in such a case. Moreover, since the quantum channels are assumed to be noninteracting and spatially well separated, the two-mode correlated attack reduces to two independent single-mode entangling cloner attacks.

Specifically, a single-mode entangling cloner attack assumes that Eve can split the incoming CV states in both channels independently using a BS with transmittance T that is equal to the loss of the Alice-Charlie and Bob-Charlie channels (assuming that the loss in both channels is the same). The two input modes for this BS correspond to the quantum state being transmitted and a vacuum state (or a thermal state if we consider thermal noise in the channels). Eve then stores the reflected states in a quantum memory, while the transmitted states are sent to Charlie via identity channels having no loss. Subsequently, Eve can then perform a joint measurement on the two retained states (corresponding to Alice-Charlie and Bob-Charlie channels) that are stored in a quantum memory and try to guess the key of Alice or Bob on the basis of the outcomes observed. However, Alice and Bob can estimate the transmission losses of their respective channels given by T. As a consequence, the maximum information that can be obtained by Eve becomes a function of the channel loss parameter T and the results publicly declared by Charlie. The information by Eve is then bounded by the Holevo bound $\chi(A:E)$.

Since Alice and Bob share the state $\rho_{a_1b_1}$ with probability P_0, the secure key rate r between Alice and Bob is then given as

$$r \geq P_0\left[I(A:B) - \chi(A:E)\right] \text{ subject to}$$
$$P_0 = \frac{\left(1-e^{-\eta_o T\alpha^2}\right)^2}{2}. \tag{E1}$$

Evaluation of the mutual information between Alice and Bob is relatively simple and is accomplished by the use of their observed joint statistics. If Alice and Bob perform a measurement corresponding to observables A and B, the mutual information between the two parties sharing a state ρ_{ab} is given as $I(A:B) = H(A) + H(B) - H(A,B)$, where $H(A)$ (and $H(B)$) is the Shannon entropy corresponding to the observable A (and B) measured on the state $\rho_a = \mathrm{tr}_b(\rho_{ab})$ and $H(A,B)$ is the Shannon entropy of the observables jointly measured on the state ρ_{ab}.

2. Calculation of $I(A:B)$ and $\chi(A:E)$

To evaluate the mutual information we first look at the final state that is shared between Alice and Bob, which is given as

$$\rho_{a_1b_1} = \frac{1}{2}\left[|01\rangle_{a_1b_1}\langle 01| + |10\rangle_{a_1b_1}\langle 10| + h\left(g\,|01\rangle_{a_1b_1} \times \langle 10| + g^*\,|10\rangle_{a_1b_1}\langle 01|\right)\right], \tag{E2}$$

where $h = e^{-4(1-T\eta_h)\alpha^2}$ and $g = e^{-4i\sqrt{T\eta_h}\alpha p}$, with the reduced states of Alice and Bob as

$$\rho_{a_1} = \rho_{b_1} = \frac{1}{2}\left(|0\rangle\langle 0| + |1\rangle\langle 1|\right). \tag{E3}$$

In the QKD protocol we consider that both Alice and Bob choose the observable $M = \sigma_Z$ to generate a key. The corresponding projective measurement can then be written as $\{\Pi_0, \Pi_1\}$, where $\Pi_0 = |0\rangle\langle 0|$ and $\Pi_1 = \mathbb{1} - \Pi_0 = |1\rangle\langle 1|$. We also consider that the photon-number detectors are imperfect, having efficiency η_d. A general m-photon detector with efficiency η_d is described by the measurement operators

$$\Pi_m(\eta_d) = \eta_d^m \sum_k (1-\eta_d)^k\,|k+m\rangle\langle k+m|. \tag{E4}$$

Because in our scheme we have only two outcomes (corresponding to Π_0 and $\mathbb{1} - \Pi_0$), an imperfect measurement

of σ_Z then corresponds to measurement operators

$$\Pi_0(\eta_d) = |0\rangle\langle 0| + (1-\eta_d)|1\rangle\langle 1|, \tag{E5a}$$

$$\Pi_1(\eta_d) = \mathbb{1} - \Pi_0 = \eta_d |1\rangle\langle 1|. \tag{E5b}$$

We first consider the imperfect measurement of σ_Z on Alice's reduced state ρ_{a_1}. The outcome $\Pi_0(\eta_d)$ occurs with probability $p_0 = \frac{1}{2}[1 + (1-\eta_d)] = (2-\eta_d)/2$, while the outcome $\Pi_1(\eta_d)$ occurs with probability $p_1 = 1 - p_0 = \eta_d/2$. As a consequence, the Shannon entropy of imperfectly measuring σ_Z on Alice's reduced state is given as

$$\begin{aligned} H(\sigma_3) &= -p_0 \log_2 p_0 - p_1 \log_2 p_1 \\ &= -\left(\frac{2-\eta_d}{2}\right)\log_2\left(\frac{2-\eta_d}{2}\right) - \frac{\eta_d}{2}\log_2\frac{\eta_d}{2}. \\ &= 1 - \frac{2-\eta_d}{2}\log_2(2-\eta_d) - \frac{\eta_d}{2}\log_2\eta_d. \end{aligned} \tag{E6}$$

Similarly, it can be seen that the same expression also holds true for the imperfect measurement of σ_Z on Bob's reduced state. The measurement operators corresponding to the case when Alice and Bob jointly (and imperfectly) measure σ_Z on their respective reduced states are

$$\begin{aligned} \Pi_{00}(\eta_d) &= |00\rangle\langle 00| + (1-\eta_d)^2 |11\rangle \\ &\quad \langle 11| + (1-\eta_d)|01\rangle\langle 01| + (1-\eta_d)|10\rangle\langle 10|, \end{aligned} \tag{E7a}$$

$$\Pi_{01}(\eta_d) = \eta_d |01\rangle\langle 01| + \eta_d(1-\eta_d)|11\rangle\langle 11|, \tag{E7b}$$

$$\Pi_{10}(\eta_d) = \eta_d |10\rangle\langle 10| + \eta_d(1-\eta_d)|11\rangle\langle 11|, \tag{E7c}$$

$$\Pi_{11}(\eta_d) = \eta_d^2 |11\rangle\langle 11|, \tag{E7d}$$

which occur with probabilities $p_{00} = 1-\eta_d$, $p_{01} = \eta_d/2$, $p_{10} = \eta_d/2$, and $p_{11} = 0$, respectively. As a consequence, the Shannon entropy for the joint measurement becomes

$$\begin{aligned} H(\sigma_Z, \sigma_Z) &= -p_{00}\log_2 p_{00} - p_{01}\log_2 p_{01} \\ &\quad - p_{10}\log_2 p_{10} - p_{11}\log_2 p_{11} \\ &= -(1-\eta_d)\log_2(1-\eta_d) - \eta_d \log_2\frac{\eta_d}{2} \\ &= \eta_d - (1-\eta_d)\log_2(1-\eta_d) - \eta_d\log_2\eta_d. \end{aligned} \tag{E8}$$

The mutual information between Alice and Bob can then be written as

$$\begin{aligned} I(A:B) &= H(\sigma_Z) + H(\sigma_Z) - H(\sigma_Z, \sigma_Z) \\ &= (2-\eta_d) - \big[(2-\eta_d)\log_2(2-\eta_d) \\ &\quad - (1-\eta_d)\log_2(1-\eta_d)\big]. \end{aligned} \tag{E9}$$

Evidently, in the absence of any imperfection ($\eta_d = 1$), one obtains perfect correlation, i.e, $\lim_{\eta_d \to 1} I(A:B) = 1$. Next we evaluate the Holevo bound $\chi(A:E)$.

To evaluate the Holevo bound, we assume that Eve has access to a purification of the state $\rho_{a_1b_1}$, which we denote by $\rho_{a_1b_1E}$, such that $\rho_e = \mathrm{tr}_{a_1b_1}(\rho_{a_1b_1e})$ is the reduced state of Eve. Moreover, we also assume that Alice's measurement outcomes are represented by rank-1 operators. Since $\rho_{a_1b_1e}$ is pure by definition, we have $S(\rho_{a_1b_1}) = S(\rho_e)$, where $S(X)$ is the von Neumann entropy of a system X. Moreover, if Alice's measurement outcomes are represented by rank-1 operators, then the reduced state of Bob and Eve conditioned on Alice's outcome x, given by $\rho_{b_1e|x}$, is also pure. Therefore, by definition of von Neumann entropy, we have $S(\rho_{e|x}) = S(\rho_{b_1|x})$, where $\rho_{b_1|x}$ is the reduced state of Bob conditioned on Alice's outcome x. In this case, the Holevo bound can then be written as [49]

$$\chi(A:E) = S(\rho_{a_1b_1}) - \sum_x p_x S\left(\rho_{b_1|x}\right). \tag{E10}$$

For the state $\rho_{a_1b_1}$ as given in Eq. (E2), its eigenvalues are given as $\lambda_\pm = 1 \pm h/2$, leading to the von Neumann entropy as

$$\begin{aligned} S(\rho_{a_1b_1}) &= -\lambda_+\log_2\lambda_+ - \lambda_-\log_2\lambda_- \\ &= -\left(\frac{1+h}{2}\right)\log_2\left(\frac{1+h}{2}\right) \\ &\quad -\left(\frac{1-h}{2}\right)\log_2\left(\frac{1-h}{2}\right) \\ &= 1 - \frac{1}{2}\big[(1+h)\log_2(1+h) \\ &\quad + (1-h)\log_2(1-h)\big]. \end{aligned} \tag{E11}$$

On the other hand, the reduced states of Bob corresponding to the two outcomes of the imperfect measurement of σ_Z by Alice are given as

$$\begin{aligned} \rho_{b_1|0} &= \frac{\mathrm{tr}_{a_1}\left[\rho_{a_1b_1}\Pi_0(\eta_d)\right]}{\mathrm{tr}\left[\rho_{a_1b_1}\Pi_0(\eta_d)\right]} \\ &= \frac{1}{2-\eta_d}\left(|1\rangle\langle 1| + (1-\eta_d)|0\rangle\langle 0|\right), \end{aligned} \tag{E12a}$$

$$\rho_{b_1|1} = \frac{\mathrm{tr}_{a_1}\left[\rho_{a_1b_1}\Pi_1(\eta_d)\right]}{\mathrm{tr}\left[\rho_{a_1b_1}\Pi_1(\eta_d)\right]} = |1\rangle\langle 1|, \tag{E12b}$$

which lead to

$$\sum_{x=0}^{1} p_x S\left(\rho_{b_1|x}\right) = \frac{2-\eta_d}{2}\left[-\left(\frac{1}{2-\eta_d}\right)\log_2\left(\frac{1}{2-\eta_d}\right) - \left(\frac{1-\eta_d}{2-\eta_d}\right)\log_2\left(\frac{1-\eta_d}{2-\eta_d}\right)\right]$$
$$= \frac{1}{2}\big[(2-\eta_d)\log_2(2-\eta_d) - (1-\eta_d)\log_2(1-\eta_d)\big]. \tag{E13}$$

As a consequence, the Holevo bound can be written as

$$\chi(A:E) = S(\rho_{a_1b_1}) - \sum_x p_x S\left(\rho_{b_1|x}\right)$$
$$= 1 - \frac{1}{2}\big[(1+h)\log_2(1+h) + (1-h)\log_2(1-h)\big] - \frac{1}{2}\big[(2-\eta_d)\log_2(2-\eta_d) - (1-\eta_d)\log_2(1-\eta_d)\big]. \tag{E14}$$

By plugging the mutual information given in Eq. (E9) and the Holevo bound, given in Eq. (E14), in the secure key rate, given by Eq. (E1), we obtain

$$r \geq p_0\left[I(A:B) - \chi(A:E)\right]$$
$$= p_0\left\{1 - \eta_d + \frac{1}{2}\big[(1+h)\log_2(1+h) + (1-h)\log_2(1-h)\big] - \frac{1}{2}\big[(2-\eta_d)\log_2(2-\eta_d) - (1-\eta_d)\log_2(1-\eta_d)\big]\right\}. \tag{E15}$$

APPENDIX F: FIDELITY BETWEEN THE HE STATES THAT PASSED THROUGH LOSS-ONLY AND LOSSY-AND-NOISY CHANNELS

In this appendix, we analyze the impact of thermal noise present in the quantum channel between Alice (Bob) and Charlie. We show that the final state after a loss-only channel is almost equivalent to the final state after passing through a channel characterized by loss and thermal noise. Using this result, we aim to reduce the complexity of the calculation by focusing only on loss-only quantum channels connecting all the parties.

1. General state after channel transmission

Let us consider that an incoming signal passes through a lossy channel having transmittance T with additional thermal noise. Mathematically, the channel transmission can be written as $U_{\rm ch} : \rho_{\rm s,in} \to \rho_{\rm s,out}$, where $\rho_{\rm s,in}$ ($\rho_{\rm s,out}$) is input (output) state of the channel. Such transmission can be modeled as follows. First, the incoming state (in mode a) is mixed with an ancilla initialized in a thermal state (in mode b) via a BS with transmittance T and two output modes. Subsequently, the output of the quantum channel is obtained by our tracing out the outgoing ancillary mode of the BS.

The action of a BS with transmittance T is described in terms of a unitary operation U_T^{ab} on the input modes a and b that leads to the transformation matrix between the input and output modes, labeled by a' and b', as

$$\begin{pmatrix}\hat{a}\\ \hat{b}\end{pmatrix} \to \begin{pmatrix}\hat{a}'\\ \hat{b}'\end{pmatrix} = \begin{pmatrix}\sqrt{T} & \sqrt{1-T}\\ -\sqrt{1-T} & \sqrt{T}\end{pmatrix}\begin{pmatrix}\hat{a}\\ \hat{b}\end{pmatrix}, \tag{F1}$$

where $\hat{a}$ corresponds to the annihilation operator for mode a and $T = 0.5$ represents a balanced (50:50) BS. As a consequence, the action of the channel on a coherent state ($|\alpha\rangle$) in mode a is described as $U_T^{ab}\,|\alpha\rangle_a \otimes |\beta\rangle_b \to |\alpha\rangle_{a'} \otimes |\beta\rangle_{b'} = |\sqrt{T}\alpha + \sqrt{1-T}\beta\rangle_a \otimes |\sqrt{T}\beta - \sqrt{1-T}\alpha\rangle_b = |\sqrt{T}\alpha + \sqrt{1-T}\beta, \sqrt{T}\beta - \sqrt{1-T}\alpha\rangle_{ab}$.

Let us consider that, in the coherent-state basis, the incoming signal is in the quantum state given by $\rho_{\rm s,in} = \int d^2\alpha/\pi (d^2\beta/\pi) C(\alpha,\beta)\,|\alpha\rangle_a\,\langle\beta|$, while the ancilla thermal state is described as $\rho_{\rm anc,th} = (1-x)\sum_k x^k\,|k\rangle_b\,\langle k| = (1-x)\int d^2\eta/\pi (d^2\zeta/\pi) e^{-((|\eta|^2+|\zeta|^2)/2)+x\eta^*\zeta}\,|\eta\rangle_b\,\langle\zeta|$, where $x = \bar{n}/(1+\bar{n})$ such that $\bar{n}$ is the average number of thermal

photons. In view of the action of a BS on the coherent states, one can easily show that

$$\begin{aligned}\rho_{\text{out}} &= U_T^{ab}\rho_{\text{s,in}}\otimes\rho_{\text{anc,th}}\left(U_T^{ab}\right)^\dagger\\ &= (1-x)\int\frac{d^2\alpha}{\pi}\frac{d^2\beta}{\pi}\frac{d^2\eta}{\pi}\frac{d^2\zeta}{\pi}C(\alpha,\beta)e^{-\frac{|\eta|^2+|\zeta|^2}{2}+x\eta^*\zeta}\left[U_T^{ab}\left|\alpha,\eta\right\rangle_{ab}\left\langle\beta,\zeta\right|\left(U_T^{ab}\right)^\dagger\right]\\ &= (1-x)\int\frac{d^2\alpha}{\pi}\frac{d^2\beta}{\pi}\frac{d^2\eta}{\pi}\frac{d^2\zeta}{\pi}C(\alpha,\beta)e^{-\frac{|\eta|^2+|\zeta|^2}{2}+x\eta^*\zeta}\left|\sqrt{T}\alpha+\sqrt{1-T}\eta,\sqrt{T}\eta-\sqrt{1-T}\alpha\right\rangle\\ &\quad\otimes\left\langle\sqrt{T}\beta+\sqrt{1-T}\zeta,\sqrt{T}\zeta-\sqrt{1-T}\beta\right|.\end{aligned}\tag{F2}$$

Consequently, the channel output signal state becomes

$$\begin{aligned}&U_{\text{ch}}:\rho_{\text{s,in}}\to\rho_{\text{s,out}}=\text{Tr}_{\text{anc}}\left(\rho_{\text{out}}\right)\\ &= (1-x)\int\frac{d^2\alpha}{\pi}\frac{d^2\beta}{\pi}\frac{d^2\eta}{\pi}\frac{d^2\zeta}{\pi}C(\alpha,\beta)e^{-\frac{|\eta|^2+|\zeta|^2}{2}+x\eta^*\zeta}\left|\sqrt{T}\alpha+\sqrt{1-T}\eta\right\rangle_a\left\langle\sqrt{T}\beta+\sqrt{1-T}\zeta\right|\\ &\quad\times\left\langle\sqrt{T}\zeta-\sqrt{1-T}\beta\left|\sqrt{T}\eta-\sqrt{1-T}\alpha\right\rangle\right.\\ &= (1-x)\int\frac{d^2\alpha}{\pi}\frac{d^2\beta}{\pi}\frac{d^2\eta}{\pi}\frac{d^2\zeta}{\pi}C(\alpha,\beta)e^{-\frac{1-T}{2}\left(|\alpha|^2+|\beta|^2\right)+(1-T)\alpha\beta^*}e^{-\frac{1+T}{2}\left(|\eta|^2+|\zeta|^2\right)+x\eta^*\zeta+T\eta\zeta^*}\\ &\quad\times e^{\sqrt{T(1-T)}\left[\frac{\alpha^*\eta+\alpha\eta^*}{2}+\frac{\beta^*\zeta+\beta\zeta^*}{2}-(\beta^*\eta+\alpha\zeta^*)\right]}\left|\sqrt{T}\alpha+\sqrt{1-T}\eta\right\rangle_a\left\langle\sqrt{T}\beta+\sqrt{1-T}\zeta\right|\\ &= (1-x)\int\frac{d^2\alpha}{\pi}\frac{d^2\beta}{\pi}\frac{d^2\eta}{\pi}\frac{d^2\zeta}{\pi}C(\alpha,\beta)e^{-\frac{1-T}{2}\left(|\alpha|^2+|\beta|^2\right)+(1-T)\alpha\beta^*}e^{-\frac{1+T}{2}\left(|\eta|^2+|\zeta|^2\right)+x\eta^*\zeta+T\eta\zeta^*}\\ &\quad\times e^{\sqrt{T(1-T)}\left[\frac{\alpha^*\eta+\alpha\eta^*}{2}+\frac{\beta^*\zeta+\beta\zeta^*}{2}-(\beta^*\eta+\alpha\zeta^*)\right]}\int\frac{d^2\lambda}{\pi}\frac{d^2\omega}{\pi}\left|\lambda\right\rangle\left\langle\omega\right|\left\langle\lambda\left|\sqrt{T}\alpha+\sqrt{1-T}\eta\right\rangle\left\langle\sqrt{T}\beta+\sqrt{1-T}\zeta\right|\omega\right\rangle\\ &= (1-x)\int\frac{d^2\alpha}{\pi}\frac{d^2\beta}{\pi}\frac{d^2\eta}{\pi}\frac{d^2\zeta}{\pi}C(\alpha,\beta)e^{-\frac{1-T}{2}\left(|\alpha|^2+|\beta|^2\right)+(1-T)\alpha\beta^*}e^{-\frac{1+T}{2}\left(|\eta|^2+|\zeta|^2\right)+x\eta^*\zeta+T\eta\zeta^*}\\ &\quad\times e^{\sqrt{T(1-T)}\left[\frac{\alpha^*\eta+\alpha\eta^*}{2}+\frac{\beta^*\zeta+\beta\zeta^*}{2}-(\beta^*\eta+\alpha\zeta^*)\right]}\int\frac{d^2\lambda}{\pi}\frac{d^2\omega}{\pi}\left|\lambda\right\rangle\left\langle\omega\right|e^{-\frac{|\lambda|^2+|\sqrt{T}\alpha+\sqrt{1-T}\eta|^2}{2}+\lambda^*\left(\sqrt{T}\alpha+\sqrt{1-T}\eta\right)}\\ &\quad\times e^{-\frac{|\omega|^2+|\sqrt{T}\beta+\sqrt{1-T}\zeta|^2}{2}+\left(\sqrt{T}\beta^*+\sqrt{1-T}\zeta^*\right)\omega}\\ &= (1-x)\int\frac{d^2\lambda}{\pi}\frac{d^2\omega}{\pi}e^{-\frac{|\lambda|^2+|\omega|^2}{2}}\left|\lambda\right\rangle\left\langle\omega\right|\int\frac{d^2\alpha}{\pi}\frac{d^2\beta}{\pi}C(\alpha,\beta)e^{-\frac{|\alpha|^2+|\beta|^2}{2}+(1-T)\alpha\beta^*+\sqrt{T}(\lambda^*\alpha+\omega\beta^*)}\\ &\quad\times\int\frac{d^2\eta}{\pi}\frac{d^2\zeta}{\pi}e^{-\left(|\eta|^2+|\zeta|^2\right)+x\eta^*\zeta+T\eta\zeta^*}e^{-\sqrt{T(1-T)}\left(\beta^*\eta+\alpha\zeta^*\right)+\sqrt{1-T}\left(\lambda^*\eta+\omega\zeta^*\right)}\\ &= \frac{1-x}{1-Tx}\int\frac{d^2\lambda}{\pi}\frac{d^2\omega}{\pi}e^{-\frac{|\lambda|^2+|\omega|^2}{2}+\frac{x(1-T)}{1-Tx}\lambda^*\omega}\left|\lambda\right\rangle\left\langle\omega\right|\int\frac{d^2\alpha}{\pi}\frac{d^2\beta}{\pi}C(\alpha,\beta)e^{-\frac{|\alpha|^2+|\beta|^2}{2}+\frac{1-T}{1-Tx}\alpha\beta^*+\frac{\sqrt{T}(1-x)}{1-Tx}(\lambda^*\alpha+\omega\beta^*)}.\end{aligned}\tag{F3}$$

In the case of a loss-only channel, i.e., in absence of additional thermal noise ($x=0$), Eq. (F3) reduces to

$$\begin{aligned}\lim_{x\to0}U_{\text{ch}}:\rho_{\text{s,in}}&\to\int\frac{d^2\alpha}{\pi}\frac{d^2\beta}{\pi}C(\alpha,\beta)e^{-\frac{1-T}{2}\left(|\alpha|^2+|\beta|^2\right)+(1-T)\alpha\beta^*}\int\frac{d^2\lambda}{\pi}\frac{d^2\omega}{\pi}e^{-\frac{|\lambda|^2+|\omega|^2+T\left(|\alpha|^2+|\beta|^2\right)}{2}+\sqrt{T}(\lambda^*\alpha+\omega\beta^*)}\left|\lambda\right\rangle\left\langle\omega\right|\\ &= \int\frac{d^2\alpha}{\pi}\frac{d^2\beta}{\pi}C(\alpha,\beta)e^{-\frac{1-T}{2}\left(|\alpha|^2+|\beta|^2\right)+(1-T)\alpha\beta^*}\int\frac{d^2\lambda}{\pi}\frac{d^2\omega}{\pi}\left|\lambda\right\rangle\left\langle\lambda\right|\left|\sqrt{T}\alpha\right\rangle\left\langle\sqrt{T}\beta\right|\left|\omega\right\rangle\left\langle\omega\right|\\ &= \int\frac{d^2\alpha}{\pi}\frac{d^2\beta}{\pi}C(\alpha,\beta)e^{-\frac{1-T}{2}\left(|\alpha|^2+|\beta|^2\right)+(1-T)\alpha\beta^*}\left|\sqrt{T}\alpha\right\rangle\left\langle\sqrt{T}\beta\right|.\end{aligned}\tag{F4}$$

2. Hybrid state after channel transmission

In our protocol, each party transmits a coherent state through a quantum channel that may have transmission loss as well as thermal noise. In the following, we evaluate all possible terms that may arise when the parties transmit the continuous-variable part through the aforementioned channel. In such a case, Eq. (F3) leads to

$$\begin{aligned}
U_{\mathrm{ch}} : |\gamma\rangle\langle\gamma| \to{}& \frac{1-x}{1-Tx}\int \frac{d^2\lambda}{\pi}\frac{d^2\omega}{\pi} e^{-\frac{|\lambda|^2+|\omega|^2}{2}+\frac{x(1-T)}{1-Tx}\lambda^*\omega} |\lambda\rangle\langle\omega| \int \frac{d^2\alpha}{\pi}\frac{d^2\beta}{\pi}\delta^2(\beta-\gamma)\,\delta^2(\alpha-\gamma) \\
&\times e^{-\frac{|\alpha|^2+|\beta|^2}{2}+\frac{1-T}{1-Tx}\alpha\beta^*+\frac{\sqrt{T}(1-x)}{1-Tx}(\lambda^*\alpha+\omega\beta^*)} \\
={}& \frac{1-x}{1-Tx}\int \frac{d^2\lambda}{\pi}\frac{d^2\omega}{\pi} e^{-\frac{|\lambda|^2+|\omega|^2}{2}+\frac{x(1-T)}{1-Tx}\lambda^*\omega} |\lambda\rangle\langle\omega| \times e^{-\frac{T(1-x)}{1-Tx}|\gamma|^2+\frac{\sqrt{T}(1-x)}{1-Tx}(\lambda^*\gamma+\omega\gamma^*)} \\
={}& e^{-\frac{T(1-x)}{1-Tx}|\gamma|^2}\frac{1-x}{1-Tx}\int \frac{d^2\lambda}{\pi}\frac{d^2\omega}{\pi} e^{-\frac{|\lambda|^2+|\omega|^2}{2}+\frac{x(1-T)}{1-Tx}\lambda^*\omega+\frac{\sqrt{T}(1-x)}{1-Tx}(\lambda^*\gamma+\omega\gamma^*)} |\lambda\rangle\langle\omega|\,,
\end{aligned} \tag{F5}$$

$$\begin{aligned}
U_{\mathrm{ch}} : |\gamma\rangle\langle-\gamma| \to{}& \frac{1-x}{1-Tx}\int \frac{d^2\lambda}{\pi}\frac{d^2\omega}{\pi} e^{-\frac{|\lambda|^2+|\omega|^2}{2}+\frac{x(1-T)}{1-Tx}\lambda^*\omega} |\lambda\rangle\langle\omega| \int \frac{d^2\alpha}{\pi}\frac{d^2\beta}{\pi}\delta^2(\beta+\gamma)\,\delta^2(\alpha-\gamma) \\
&\times e^{-\frac{|\alpha|^2+|\beta|^2}{2}+\frac{1-T}{1-Tx}\alpha\beta^*+\frac{\sqrt{T}(1-x)}{1-Tx}(\lambda^*\alpha+\omega\beta^*)} \\
={}& \frac{1-x}{1-Tx}\int \frac{d^2\lambda}{\pi}\frac{d^2\omega}{\pi} e^{-\frac{|\lambda|^2+|\omega|^2}{2}+\frac{x(1-T)}{1-Tx}\lambda^*\omega} |\lambda\rangle\langle\omega| \times e^{-\frac{T(1-x)}{1-Tx}|\gamma|^2+\frac{\sqrt{T}(1-x)}{1-Tx}(\lambda^*\gamma-\omega\gamma^*)} \\
={}& e^{-\frac{T(1-x)}{1-Tx}|\gamma|^2}\frac{1-x}{1-Tx}\int \frac{d^2\lambda}{\pi}\frac{d^2\omega}{\pi} e^{-\frac{|\lambda|^2+|\omega|^2}{2}+\frac{x(1-T)}{1-Tx}\lambda^*\omega+\frac{\sqrt{T}(1-x)}{1-Tx}(\lambda^*\gamma-\omega\gamma^*)} |\lambda\rangle\langle\omega|\,,
\end{aligned} \tag{F6}$$

$$\begin{aligned}
U_{\mathrm{ch}} : |-\gamma\rangle\langle\gamma| \to{}& \frac{1-x}{1-Tx}\int \frac{d^2\lambda}{\pi}\frac{d^2\omega}{\pi} e^{-\frac{|\lambda|^2+|\omega|^2}{2}+\frac{x(1-T)}{1-Tx}\lambda^*\omega} |\lambda\rangle\langle\omega| \int \frac{d^2\alpha}{\pi}\frac{d^2\beta}{\pi}\delta^2(\beta-\gamma)\,\delta^2(\alpha+\gamma) \\
&\times e^{-\frac{|\alpha|^2+|\beta|^2}{2}+\frac{1-T}{1-Tx}\alpha\beta^*+\frac{\sqrt{T}(1-x)}{1-Tx}(\lambda^*\alpha+\omega\beta^*)} \\
={}& \frac{1-x}{1-Tx}\int \frac{d^2\lambda}{\pi}\frac{d^2\omega}{\pi} e^{-\frac{|\lambda|^2+|\omega|^2}{2}+\frac{x(1-T)}{1-Tx}\lambda^*\omega} |\lambda\rangle\langle\omega| \times e^{-\frac{T(1-x)}{1-Tx}|\gamma|^2+\frac{\sqrt{T}(1-x)}{1-Tx}(-\lambda^*\gamma+\omega\gamma^*)} \\
={}& e^{-\frac{T(1-x)}{1-Tx}|\gamma|^2}\frac{1-x}{1-Tx}\int \frac{d^2\lambda}{\pi}\frac{d^2\omega}{\pi} e^{-\frac{|\lambda|^2+|\omega|^2}{2}+\frac{x(1-T)}{1-Tx}\lambda^*\omega-\frac{\sqrt{T}(1-x)}{1-Tx}(\lambda^*\gamma-\omega\gamma^*)} |\lambda\rangle\langle\omega|\,,
\end{aligned} \tag{F7}$$

$$\begin{aligned}
U_{\mathrm{ch}} : |-\gamma\rangle\langle-\gamma| \to{}& \frac{1-x}{1-Tx}\int \frac{d^2\lambda}{\pi}\frac{d^2\omega}{\pi} e^{-\frac{|\lambda|^2+|\omega|^2}{2}+\frac{x(1-T)}{1-Tx}\lambda^*\omega} |\lambda\rangle\langle\omega| \int \frac{d^2\alpha}{\pi}\frac{d^2\beta}{\pi}\delta^2(\beta+\gamma)\,\delta^2(\alpha+\gamma) \\
&\times e^{-\frac{|\alpha|^2+|\beta|^2}{2}+\frac{1-T}{1-Tx}\alpha\beta^*+\frac{\sqrt{T}(1-x)}{1-Tx}(\lambda^*\alpha+\omega\beta^*)} \\
={}& \frac{1-x}{1-Tx}\int \frac{d^2\lambda}{\pi}\frac{d^2\omega}{\pi} e^{-\frac{|\lambda|^2+|\omega|^2}{2}+\frac{x(1-T)}{1-Tx}\lambda^*\omega} |\lambda\rangle\langle\omega| \times e^{-\frac{T(1-x)}{1-Tx}|\gamma|^2-\frac{\sqrt{T}(1-x)}{1-Tx}(\lambda^*\gamma+\omega\gamma^*)} \\
={}& e^{-\frac{T(1-x)}{1-Tx}|\gamma|^2}\frac{1-x}{1-Tx}\int \frac{d^2\lambda}{\pi}\frac{d^2\omega}{\pi} e^{-\frac{|\lambda|^2+|\omega|^2}{2}+\frac{x(1-T)}{1-Tx}\lambda^*\omega-\frac{\sqrt{T}(1-x)}{1-Tx}(\lambda^*\gamma+\omega\gamma^*)} |\lambda\rangle\langle\omega|\,.
\end{aligned} \tag{F8}$$

An HE state (A7) is defined as

$$|\psi\rangle_{\mathrm{HE}} = \frac{1}{\sqrt{2}}\left(|0,\alpha\rangle + |1,-\alpha\rangle\right), \tag{F9}$$

for which the multiphoton coherent-state part is transmitted through a general (both lossy and noisy) channel. From the results obtained above, it can be seen that, after the transmission, the final state is

$$\begin{aligned}\rho^{\mathrm{ch,HE}}(T,x) &= U_{\mathrm{ch}} : \rho_{\mathrm{HE}} = U_{\mathrm{ch}} : \frac{1}{2}\left(|0\rangle\langle 0| \otimes |\alpha\rangle\langle\alpha| + |0\rangle\langle 1| \otimes |\alpha\rangle\langle -\alpha| + |1\rangle\langle 0| \otimes |-\alpha\rangle\langle\alpha| + |1\rangle\langle 1| \otimes |-\alpha\rangle\langle -\alpha|\right) \\ &= \frac{e^{-\frac{T(1-x)}{1-Tx}|\alpha|^2}}{2}\frac{1-x}{1-Tx}\int \frac{d^2\lambda}{\pi}\frac{d^2\omega}{\pi} e^{-\frac{|\lambda|^2+|\omega|^2}{2}+\frac{x(1-T)}{1-Tx}\lambda^*\omega}|\lambda\rangle\langle\omega| \\ &\otimes\Big[e^{\frac{\sqrt{T}(1-x)}{1-Tx}(\lambda^*\alpha+\omega\alpha^*)}|0\rangle\langle 0| + e^{\frac{\sqrt{T}(1-x)}{1-Tx}(\lambda^*\alpha-\omega\alpha^*)}|0\rangle\langle 1| + e^{-\frac{\sqrt{T}(1-x)}{1-Tx}(\lambda^*\alpha-\omega\alpha^*)}|1\rangle\langle 0| \\ &+ e^{-\frac{\sqrt{T}(1-x)}{1-Tx}(\lambda^*\alpha+\omega\alpha^*)}|1\rangle\langle 1|\Big]. \end{aligned} \tag{F10}$$

3. HE state at Charlie's end after transmission through a loss-only channel and a general channel

Let us consider that Alice and Bob prepare their individual HE states $|\psi\rangle_{a_1a_2}$ and $|\psi\rangle_{b_1b_2}$ as

$$|\psi\rangle_{a_1a_2} = \frac{1}{\sqrt{2}}\left(|0,\alpha\rangle_{a_1a_2} + |1,-\alpha\rangle_{a_1a_2}\right), \tag{F11a}$$

$$|\psi\rangle_{b_1b_2} = \frac{1}{\sqrt{2}}\left(|0,\alpha\rangle_{b_1b_2} + |1,-\alpha\rangle_{b_1b_2}\right), \tag{F11b}$$

where $|0,\alpha\rangle_{a_1a_2} = |0\rangle_{a_1}|\alpha\rangle_{a_2}$. Using Eq. (F10), one can show that the total four-mode state at the input of Charlie after it has passed through a general channel is given by

$$\begin{aligned}\rho_{\mathrm{in,tot}}(T,x) &= \rho^{\mathrm{ch}}_{a_1a_2}\otimes\rho^{\mathrm{ch}}_{b_1b_2} \\ &= \frac{e^{-\frac{2T(1-x)}{1-Tx}|\alpha|^2}}{4}\left(\frac{1-x}{1-Tx}\right)^2\int\frac{d^2\lambda}{\pi}\frac{d^2\omega}{\pi}\frac{d^2\chi}{\pi}\frac{d^2\xi}{\pi}e^{-\frac{|\lambda|^2+|\omega|^2+|\chi|^2+|\xi|^2}{2}+\frac{x(1-T)}{1-Tx}(\lambda^*\omega+\chi^*\xi)}|\lambda\rangle_{a_2}\langle\omega|\otimes|\chi\rangle_{b_2}\langle\xi| \\ &\otimes\Big[e^{\frac{\sqrt{T}(1-x)}{1-Tx}(\lambda^*\alpha+\omega\alpha^*)}|0\rangle_{a_1}\langle 0| + e^{\frac{\sqrt{T}(1-x)}{1-Tx}(\lambda^*\alpha-\omega\alpha^*)}|0\rangle_{a_1}\langle 1| \\ &+ e^{-\frac{\sqrt{T}(1-x)}{1-Tx}(\lambda^*\alpha-\omega\alpha^*)}|1\rangle_{a_1}\langle 0| + e^{-\frac{\sqrt{T}(1-x)}{1-Tx}(\lambda^*\alpha+\omega\alpha^*)}|1\rangle_{a_1}\langle 1|\Big] \\ &\otimes\Big[e^{\frac{\sqrt{T}(1-x)}{1-Tx}(\chi^*\alpha+\xi\alpha^*)}|0\rangle_{b_1}\langle 0| + e^{\frac{\sqrt{T}(1-x)}{1-Tx}(\chi^*\alpha-\xi\alpha^*)}|0\rangle_{b_1}\langle 1| \\ &+ e^{-\frac{\sqrt{T}(1-x)}{1-Tx}(\chi^*\alpha-\xi\alpha^*)}|1\rangle_{b_1}\langle 0| + e^{-\frac{\sqrt{T}(1-x)}{1-Tx}(\chi^*\alpha+\xi\alpha^*)}|1\rangle_{b_1}\langle 1|\Big] \\ &= \frac{e^{-\frac{2T(1-x)}{1-Tx}|\alpha|^2}}{4}\left(\frac{1-x}{1-Tx}\right)^2\int\frac{d^2\lambda}{\pi}\frac{d^2\omega}{\pi}\frac{d^2\chi}{\pi}\frac{d^2\xi}{\pi}e^{-\frac{|\lambda|^2+|\omega|^2+|\chi|^2+|\xi|^2}{2}+\frac{x(1-T)}{1-Tx}(\lambda^*\omega+\chi^*\xi)}|\lambda,\chi\rangle_{a_2b_2}\langle\omega,\xi| \\ &\otimes\Big[\Big(e^{\frac{\sqrt{T}(1-x)}{1-Tx}[(\lambda^*+\chi^*)\alpha+(\omega+\xi)\alpha^*]}|0,0\rangle_{a_1b_1}\langle 0,0| + e^{\frac{\sqrt{T}(1-x)}{1-Tx}[(\lambda^*+\chi^*)\alpha+(\omega-\xi)\alpha^*]}|0,0\rangle_{a_1b_1}\langle 0,1| \\ &+ e^{\frac{\sqrt{T}(1-x)}{1-Tx}[(\lambda^*-\chi^*)\alpha+(\omega+\xi)\alpha^*]}|0,1\rangle_{a_1b_1}\langle 0,0| + e^{\frac{\sqrt{T}(1-x)}{1-Tx}[(\lambda^*-\chi^*)\alpha+(\omega-\xi)\alpha^*]}|0,1\rangle_{a_1b_1}\langle 0,1|\Big) \\ &+ \Big(e^{\frac{\sqrt{T}(1-x)}{1-Tx}[(\lambda^*+\chi^*)\alpha-(\omega-\xi)\alpha^*]}|0,0\rangle_{a_1b_1}\langle 1,0| + e^{\frac{\sqrt{T}(1-x)}{1-Tx}[(\lambda^*+\chi^*)\alpha-(\omega+\xi)\alpha^*]}|0,0\rangle_{a_1b_1}\langle 1,1| \\ &+ e^{\frac{\sqrt{T}(1-x)}{1-Tx}[(\lambda^*-\chi^*)\alpha-(\omega-\xi)\alpha^*]}|0,1\rangle_{a_1b_1}\langle 1,0| + e^{\frac{\sqrt{T}(1-x)}{1-Tx}[(\lambda^*-\chi^*)\alpha-(\omega+\xi)\alpha^*]}|0,1\rangle_{a_1b_1}\langle 1,1|\Big)\end{aligned}$$

$$+\Big(e^{-\frac{\sqrt{T}(1-x)}{1-Tx}\left[(\lambda^*-\chi^*)\alpha-(\omega+\xi)\alpha^*\right]}|1,0\rangle_{a_1b_1}\langle 0,0|+e^{-\frac{\sqrt{T}(1-x)}{1-Tx}\left[(\lambda^*-\chi^*)\alpha-(\omega-\xi)\alpha^*\right]}|1,0\rangle_{a_1b_1}\langle 0,1|$$
$$+e^{-\frac{\sqrt{T}(1-x)}{1-Tx}\left[(\lambda^*+\chi^*)\alpha-(\omega+\xi)\alpha^*\right]}|1,1\rangle_{a_1b_1}\langle 0,0|+e^{-\frac{\sqrt{T}(1-x)}{1-Tx}\left[(\lambda^*+\chi^*)\alpha-(\omega-\xi)\alpha^*\right]}|1,1\rangle_{a_1b_1}\langle 0,1|\Big)$$
$$+\Big(e^{-\frac{\sqrt{T}(1-x)}{1-Tx}\left[(\lambda^*-\chi^*)\alpha+(\omega-\xi)\alpha^*\right]}|1,0\rangle_{a_1b_1}\langle 1,0|+e^{-\frac{\sqrt{T}(1-x)}{1-Tx}\left[(\lambda^*-\chi^*)\alpha+(\omega+\xi)\alpha^*\right]}|1,0\rangle_{a_1b_1}\langle 1,1|$$
$$+e^{-\frac{\sqrt{T}(1-x)}{1-Tx}\left[(\lambda^*+\chi^*)\alpha+(\omega-\xi)\alpha^*\right]}|1,1\rangle_{a_1b_1}\langle 1,0|+e^{-\frac{\sqrt{T}(1-x)}{1-Tx}\left[(\lambda^*+\chi^*)\alpha+(\omega+\xi)\alpha^*\right]}|1,1\rangle_{a_1b_1}\langle 1,1|\Big)\Big]. \tag{F12}$$

In the absence of the additional thermal noise ($x \to 0$) the transmission channel simply becomes a loss-only channel and the state at the input of Charlie (after transmission) can be written as

$$\rho_{\text{in,tot}}(T) = \lim_{x\to 0}\rho_{\text{in,tot}}(T,x)$$
$$= \frac{e^{-2T|\alpha|^2}}{4}\int\frac{d^2\lambda}{\pi}\frac{d^2\omega}{\pi}\frac{d^2\chi}{\pi}\frac{d^2\xi}{\pi}e^{-\frac{|\lambda|^2+|\omega|^2+|\chi|^2+|\xi|^2}{2}}|\lambda,\chi\rangle_{a_2b_2}\langle\omega,\xi|$$
$$\otimes\Big[\Big(e^{\sqrt{T}\left[(\lambda^*+\chi^*)\alpha+(\omega+\xi)\alpha^*\right]}|0,0\rangle_{a_1b_1}\langle 0,0|+e^{\sqrt{T}\left[(\lambda^*+\chi^*)\alpha+(\omega-\xi)\alpha^*\right]}|0,0\rangle_{a_1b_1}\langle 0,1|$$
$$+e^{\sqrt{T}\left[(\lambda^*-\chi^*)\alpha+(\omega+\xi)\alpha^*\right]}|0,1\rangle_{a_1b_1}\langle 0,0|+e^{\sqrt{T}\left[(\lambda^*-\chi^*)\alpha+(\omega-\xi)\alpha^*\right]}|0,1\rangle_{a_1b_1}\langle 0,1|\Big)$$
$$+\Big(e^{\sqrt{T}\left[(\lambda^*+\chi^*)\alpha-(\omega+\xi)\alpha^*\right]}|0,0\rangle_{a_1b_1}\langle 1,0|+e^{\sqrt{T}\left[(\lambda^*+\chi^*)\alpha-(\omega-\xi)\alpha^*\right]}|0,0\rangle_{a_1b_1}\langle 1,1|$$
$$+e^{\sqrt{T}\left[(\lambda^*-\chi^*)\alpha-(\omega+\xi)\alpha^*\right]}|0,1\rangle_{a_1b_1}\langle 1,0|+e^{\sqrt{T}\left[(\lambda^*-\chi^*)\alpha-(\omega-\xi)\alpha^*\right]}|0,1\rangle_{a_1b_1}\langle 1,1|\Big)$$
$$+\Big(e^{-\sqrt{T}\left[(\lambda^*-\chi^*)\alpha-(\omega+\xi)\alpha^*\right]}|1,0\rangle_{a_1b_1}\langle 0,0|+e^{-\sqrt{T}\left[(\lambda^*-\chi^*)\alpha-(\omega-\xi)\alpha^*\right]}|1,0\rangle_{a_1b_1}\langle 0,1|$$
$$+e^{-\sqrt{T}\left[(\lambda^*+\chi^*)\alpha-(\omega+\xi)\alpha^*\right]}|1,1\rangle_{a_1b_1}\langle 0,0|+e^{-\sqrt{T}\left[(\lambda^*+\chi^*)\alpha-(\omega-\xi)\alpha^*\right]}|1,1\rangle_{a_1b_1}\langle 0,1|\Big)$$
$$+\Big(e^{-\sqrt{T}\left[(\lambda^*-\chi^*)\alpha+(\omega-\xi)\alpha^*\right]}|1,0\rangle_{a_1b_1}\langle 1,0|+e^{-\sqrt{T}\left[(\lambda^*-\chi^*)\alpha+(\omega+\xi)\alpha^*\right]}|1,0\rangle_{a_1b_1}\langle 1,1|$$
$$+e^{-\sqrt{T}\left[(\lambda^*+\chi^*)\alpha+(\omega-\xi)\alpha^*\right]}|1,1\rangle_{a_1b_1}\langle 1,0|+e^{-\sqrt{T}\left[(\lambda^*+\chi^*)\alpha+(\omega+\xi)\alpha^*\right]}|1,1\rangle_{a_1b_1}\langle 1,1|\Big)\Big]. \tag{F13}$$

4. Fidelity between HE states at Charlie's end after transmission through a loss-only channel and a general channel

In this subsection, we evaluate how different the state given in Eq. (F12) is from the state given in Eq. (F13) for a given loss and thermal noise. To estimate it, we evaluate the fidelity between the states given by Eqs. (F12) and (F13) as

$$F = \text{tr}\left[\rho_{\text{in,tot}}(\text{T})\rho_{\text{in,tot}}(\text{T},\text{x})\right]$$
$$= \frac{e^{-2T\frac{2-x(1+T)}{1-Tx}|\alpha|^2}}{16}\left(\frac{1-x}{1-Tx}\right)^2$$
$$\times\int\frac{d^2\Lambda_i}{\pi^8}e^{-\left(|\lambda_1|^2+|\omega_1|^2+|\chi_1|^2+|\xi_1|^2+|\lambda_2|^2+|\omega_2|^2+|\chi_2|^2+|\xi_2|^2\right)+\left(\omega_2^*\lambda_1+\xi_2^*\chi_1+\omega_1^*\lambda_2+\xi_1^*\chi_2\right)}$$
$$\times\Big[\Big(e^{\frac{\sqrt{T}(1-x)}{1-Tx}\left[(\lambda_1^*+\chi_1^*)\alpha+(\omega_1+\xi)\alpha_1^*\right]+\sqrt{T}\left[(\lambda_2^*+\chi_2^*)\alpha+(\omega_2+\xi_2)\alpha^*\right]}+e^{\frac{\sqrt{T}(1-x)}{1-Tx}\left[(\lambda_1^*+\chi_1^*)\alpha+(\omega_1-\xi)\alpha_1^*\right]+\sqrt{T}\left[(\lambda_2^*-\chi_2^*)\alpha+(\omega_2+\xi_2)\alpha^*\right]}$$
$$+e^{\frac{\sqrt{T}(1-x)}{1-Tx}\left[(\lambda_1^*-\chi_1^*)\alpha+(\omega_1+\xi)\alpha_1^*\right]+\sqrt{T}\left[(\lambda_2^*+\chi_2^*)\alpha+(\omega_2-\xi_2)\alpha^*\right]}+e^{\frac{\sqrt{T}(1-x)}{1-Tx}\left[(\lambda_1^*-\chi_1^*)\alpha+(\omega_1-\xi)\alpha_1^*\right]+\sqrt{T}\left[(\lambda_2^*-\chi_2^*)\alpha+(\omega_2-\xi_2)\alpha^*\right]}\Big)$$

$$
\begin{aligned}
&+\left(e^{\frac{\sqrt{T}(1-x)}{1-Tx}\left[(\lambda_1^*+\chi_1^*)\alpha-(\omega_1-\xi_1)\alpha^*\right]-\sqrt{T}\left[(\lambda_2^*-\chi_2^*)\alpha-(\omega_2+\xi_2)\alpha^*\right]}+e^{\frac{\sqrt{T}(1-x)}{1-Tx}\left[(\lambda_1^*+\chi_1^*)\alpha-(\omega_1+\xi_1)\alpha^*\right]-\sqrt{T}\left[(\lambda_2^*+\chi_2^*)\alpha-(\omega_2+\xi_2)\alpha^*\right]}\right.\\
&\left.+e^{\frac{\sqrt{T}(1-x)}{1-Tx}\left[(\lambda_1^*-\chi_1^*)\alpha-(\omega_1-\xi_1)\alpha^*\right]-\sqrt{T}\left[(\lambda_2^*-\chi_2^*)\alpha-(\omega_2-\xi_2)\alpha^*\right]}+e^{\frac{\sqrt{T}(1-x)}{1-Tx}\left[(\lambda_1^*-\chi_1^*)\alpha-(\omega_1+\xi_1)\alpha^*\right]-\sqrt{T}\left[(\lambda_2^*+\chi_2^*)\alpha-(\omega_2-\xi_2)\alpha^*\right]}\right)\\
&+\left(e^{-\frac{\sqrt{T}(1-x)}{1-Tx}\left[(\lambda_1^*-\chi_1^*)\alpha-(\omega_1+\xi_1)\alpha^*\right]+\sqrt{T}\left[(\lambda_2^*+\chi_2^*)\alpha-(\omega_2-\xi_2)\alpha^*\right]}+e^{-\frac{\sqrt{T}(1-x)}{1-Tx}\left[(\lambda_1^*-\chi_1^*)\alpha-(\omega_1-\xi_1)\alpha^*\right]+\sqrt{T}\left[(\lambda_2^*-\chi_2^*)\alpha-(\omega_2-\xi_2)\alpha^*\right]}\right.\\
&\left.+e^{-\frac{\sqrt{T}(1-x)}{1-Tx}\left[(\lambda_1^*+\chi_1^*)\alpha-(\omega_1+\xi_1)\alpha^*\right]+\sqrt{T}\left[(\lambda_2^*+\chi_2^*)\alpha-(\omega_2+\xi_2)\alpha^*\right]}+e^{-\frac{\sqrt{T}(1-x)}{1-Tx}\left[(\lambda_1^*+\chi_1^*)\alpha-(\omega_1-\xi_1)\alpha^*\right]+\sqrt{T}\left[(\lambda_2^*-\chi_2^*)\alpha-(\omega_2+\xi_2)\alpha^*\right]}\right)\\
&+\left(e^{-\frac{\sqrt{T}(1-x)}{1-Tx}\left[(\lambda_1^*-\chi_1^*)\alpha+(\omega_1-\xi_1)\alpha^*\right]-\sqrt{T}\left[(\lambda_2^*-\chi_2^*)\alpha+(\omega_2-\xi_2)\alpha^*\right]}+e^{-\frac{\sqrt{T}(1-x)}{1-Tx}\left[(\lambda_1^*-\chi_1^*)\alpha+(\omega_1+\xi_1)\alpha^*\right]-\sqrt{T}\left[(\lambda_2^*+\chi_2^*)\alpha+(\omega_2-\xi_2)\alpha^*\right]}\right.\\
&\left.+e^{-\frac{\sqrt{T}(1-x)}{1-Tx}\left[(\lambda_1^*+\chi_1^*)\alpha+(\omega_1-\xi_1)\alpha^*\right]-\sqrt{T}\left[(\lambda_2^*-\chi_2^*)\alpha+(\omega_2+\xi_2)\alpha^*\right]}+e^{-\frac{\sqrt{T}(1-x)}{1-Tx}\left[(\lambda_1^*+\chi_1^*)\alpha+(\omega_1+\xi_1)\alpha^*\right]-\sqrt{T}\left[(\lambda_2^*+\chi_2^*)\alpha+(\omega_2+\xi_2)\alpha^*\right]}\right)\Bigg],
\end{aligned}
\tag{F14}
$$

where $d^2\Lambda_i = d^2\lambda_i d^2\omega_i d^2\chi_i d^2\xi_i$ $(i = 1, 2)$.

Let us now consider a generic integral as

$$
\begin{aligned}
I_1 &= \frac{e^{-2T\frac{2-x(1+T)}{1-Tx}|\alpha|^2}}{16}\left(\frac{1-x}{1-Tx}\right)^2\int\frac{d^2\Lambda_i}{\pi^8}e^{-\left(|\lambda_1|^2+|\omega_1|^2+|\chi_1|^2+|\xi_1|^2+|\lambda_2|^2+|\omega_2|^2+|\chi_2|^2+|\xi_2|^2\right)+\left(\omega_2^*\lambda_1+\xi_2^*\chi_1+\omega_1^*\lambda_2+\xi_1^*\chi_2\right)}\\
&\quad\times e^{\left[(A_1\lambda_1^*+B_1\chi_1^*)\alpha+(C_1\omega_1+D_1\xi_1)\alpha_1^*\right]+\left[(A_2\lambda_2^*+B_2\chi_2^*)\alpha+(C_2\omega_2+D_2\xi_2)\alpha^*\right]}\\
&= \frac{e^{-2T\frac{2-x(1+T)}{1-Tx}|\alpha|^2}}{16}\left(\frac{1-x}{1-Tx}\right)^2\int\frac{d^2\lambda_1}{\pi}\frac{d^2\omega_1}{\pi}\frac{d^2\chi_1}{\pi}\frac{d^2\xi_1}{\pi}e^{-\left(|\lambda_1|^2+|\omega_1|^2+|\chi_1|^2+|\xi_1|^2\right)+(A_1\lambda_1^*+B_1\chi_1^*)\alpha+(C_1\omega_1+D_1\xi_1)\alpha_1^*}\\
&\quad\times\int\frac{d^2\lambda_2}{\pi}\frac{d^2\omega_2}{\pi}\frac{d^2\chi_2}{\pi}\frac{d^2\xi_2}{\pi}e^{-\left(|\lambda_2|^2+|\omega_2|^2+|\chi_2|^2+|\xi_2|^2\right)+\left(\omega_2^*\lambda_1+\xi_2^*\chi_1+\omega_1^*\lambda_2+\xi_1^*\chi_2\right)+(A_2\lambda_2^*+B_2\chi_2^*)\alpha+(C_2\omega_2+D_2\xi_2)\alpha^*}\\
&= \frac{e^{-2T\frac{2-x(1+T)}{1-Tx}|\alpha|^2}}{16}\left(\frac{1-x}{1-Tx}\right)^2\int\frac{d^2\lambda_1}{\pi}\frac{d^2\omega_1}{\pi}\frac{d^2\chi_1}{\pi}\frac{d^2\xi_1}{\pi}e^{-\left(|\lambda_1|^2+|\omega_1|^2+|\chi_1|^2+|\xi_1|^2\right)+(A_1\lambda_1^*+B_1\chi_1^*)\alpha+(C_1\omega_1+D_1\xi_1)\alpha_1^*}\\
&\quad\times e^{(A_2\omega_1^*+B_2\xi_1^*)\alpha+(C_2\lambda_1+D_2\chi_1)\alpha^*}\\
&= \frac{e^{-2T\frac{2-x(1+T)}{1-Tx}|\alpha|^2}}{16}\left(\frac{1-x}{1-Tx}\right)^2 e^{[(A_1C_2+A_2C_1)+(B_1D_2+B_2D_1)]|\alpha|^2}.
\end{aligned}
\tag{F15}
$$

Using the result of the generic integral (F15), we get from (F14)

$$
\begin{aligned}
F &= \frac{e^{-2T\frac{2-x(1+T)}{1-Tx}|\alpha|^2}}{16}\left(\frac{1-x}{1-Tx}\right)^2\times 16e^{4T\frac{(1-x)}{1-Tx}}\\
&= e^{-\frac{2Tx(1-T)}{1-Tx}|\alpha|^2}\left(\frac{1-x}{1-Tx}\right)^2.
\end{aligned}
\tag{F16}
$$

This analysis is important because a fully general calculation, in which we consider the quantum channels to be characterized by transmission loss and thermal noise, is far more involved and lengthy to perform than if we consider the quantum channels to be characterized by transmission loss only. This can be seen from the form of the four-mode states at Charlie's input before the entanglement-swapping operation. In view of the result represented in Fig. 7, we believe that the consideration of such a general channel may not yield a result significantly different from the consideration of a loss-only channel but at the cost of a very difficult, lengthy, and complicated calculation. It may be noted that in the case of a loss-only channel, the ancilla thermal state is replaced by a vacuum state. This simplifies the calculation greatly as now we can proceed with a pure-state approach in which the total state is a pure state. In this case, it is possible to take a partial trace over the ancilla after Charlie's operations. This simplifies the overall calculation. However, such a simplification is not possible when we consider an ancilla in the thermal state, for which the overall state is mixed. This increases the number of

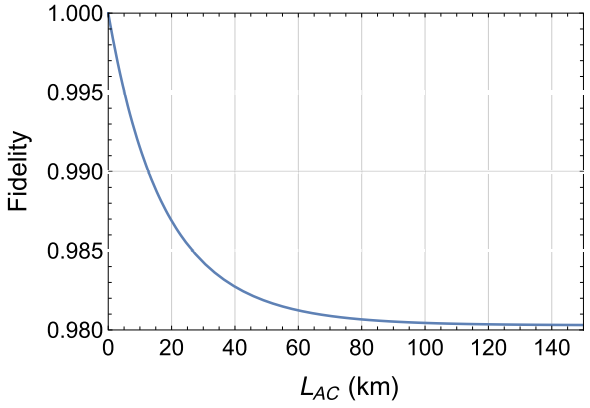

FIG. 7. Dependence of fidelity between the states obtained from the initial HE state after transmission through loss-only and lossy-and-noisy channels.

terms to be calculated by 4 times in comparison with the pure-state approach.

[1] B. Hensen, H. Bernien, A. E. Dréau, A. Reiserer, N. Kalb, M. S. Blok, J. Ruitenberg, R. F. L. Vermeulen, R. N. Schouten, C. Abellán, W. Amaya, V. Pruneri, M. W. Mitchell, M. Markham, D. J. Twitchen, D. Elkouss, S. Wehner, T. H. Taminiau, and R. Hanson, Loophole-free Bell inequality violation using electron spins separated by 1.3 kilometres, Nature (London) **526**, 682 (2015).

[2] W. Rosenfeld, D. Burchardt, R. Garthoff, K. Redeker, N. Ortegel, M. Rau, and H. Weinfurter, Event-ready Bell test using entangled atoms simultaneously closing detection and locality loopholes, Phys. Rev. Lett. **119**, 010402 (2017).

[3] B. Wittmann, S. Ramelow, F. Steinlechner, N. K. Langford, N. Brunner, H. M. Wiseman, R. Ursin, and A. Zeilinger, Loophole-free Einstein–Podolsky–Rosen experiment via quantum steering, New J. Phys. **14**, 053030 (2012).

[4] X.-S. Ma, T. Herbst, T. Scheidl, D. Wang, S. Kropatschek, W. Naylor, B. Wittmann, A. Mech, J. Kofler, E. Anisimova, V. Makarov, T. Jennewein, R. Ursin, and A. Zeilinger, Quantum teleportation over 143 kilometres using active feed-forward, Nature (London) **489**, 269 (2012).

[5] D. P. Nadlinger, P. Drmota, B. C. Nichol, G. Araneda, D. Main, R. Srinivas, D. M. Lucas, C. J. Ballance, K. Ivanov, E. Y. Z. Tan, P. Sekatski, R. L. Urbanke, R. Renner, N. Sangouard, and J.-D. Bancal, Experimental quantum key distribution certified by Bell's theorem, Nature (London) **607**, 682 (2022).

[6] W. Zhang, T. van Leent, K. Redeker, R. Garthoff, R. Schwonnek, F. Fertig, S. Eppelt, W. Rosenfeld, V. Scarani, C. C. W. Lim, and H. Weinfurter, A device-independent quantum key distribution system for distant users, Nature **607**, 687 (2022).

[7] W.-Z. Liu, Y.-Z. Zhang, Y.-Z. Zhen, M.-H. Li, Y. Liu, J. Fan, F. Xu, Q. Zhang, and J.-W. Pan, Toward a photonic demonstration of device-independent quantum key distribution, Phys. Rev. Lett. **129**, 050502 (2022).

[8] N. Gisin, S. Pironio, and N. Sangouard, Proposal for implementing device-independent quantum key distribution based on a heralded qubit amplifier, Phys. Rev. Lett. **105**, 070501 (2010).

[9] A. Cabello and F. Sciarrino, Loophole-free bell test based on local precertification of photon's presence, Phys. Rev. X **2**, 021010 (2012).

[10] E. Meyer-Scott, D. McCloskey, K. Gołos, J. Z. Salvail, K. A. G. Fisher, D. R. Hamel, A. Cabello, K. J. Resch, and T. Jennewein, Certifying the presence of a photonic qubit by splitting it in two, Phys. Rev. Lett. **116**, 070501 (2016).

[11] A. Z. Leger, S. Gambhir, J. Légère, and D. R. Hamel, Amplification of cascaded down-conversion by reusing photons with a switchable cavity, Phys. Rev. Res. **5**, 023131 (2023).

[12] E. Diamanti, H.-K. Lo, B. Qi, and Z. Yuan, Practical challenges in quantum key distribution, npj Quantum Inf. **2**, 16025 (2016).

[13] F. Xu, M. Curty, B. Qi, L. Qian, and H.-K. Lo, Discrete and continuous variables for measurement-device-independent quantum cryptography, Nat. Photonics **9**, 772 (2015).

[14] S. Pirandola, C. Ottaviani, G. Spedalieri, C. Weedbrook, S. L. Braunstein, S. Lloyd, T. Gehring, C. S. Jacobsen, and U. L. Andersen, Reply to "discrete and continuous variables for measurement-device-independent quantum cryptography", Nat. Photonics **9**, 773 (2015).

[15] C. Kumar, J. Singh, S. Bose, and Arvind, Coherence-assisted non-Gaussian measurement-device-independent quantum key distribution, Phys. Rev. A **100**, 052329 (2019).

[16] J. Singh and S. Bose, Non-Gaussian operations in measurement-device-independent quantum key distribution, Phys. Rev. A **104**, 052605 (2021).

[17] H. Jeong, Using weak nonlinearity under decoherence for macroscopic entanglement generation and quantum computation, Phys. Rev. A **72**, 034305 (2005).

[18] Y. Li, H. Jing, and M.-S. Zhan, Optical generation of a hybrid entangled state via an entangling single-photon-added coherent state, J. Phys. B: At. Mol. Opt. Phys. **39**, 2107 (2006).

[19] J.-Q. Liao, Y. Guo, H.-S. Zeng, and L.-M. Kuang, Preparation of hybrid entangled states and entangled coherent states for a single trapped ion in a cavity, J. Phys. B: At. Mol. Opt. Phys. **39**, 4709 (2006).

[20] B. He, Q. Lin, and C. Simon, Cross-Kerr nonlinearity between continuous-mode coherent states and single photons, Phys. Rev. A **83**, 053826 (2011).

[21] M. Hosseini, S. Rebic, B. M. Sparkes, J. Twamley, B. C. Buchler, and P. K. Lam, Memory-enhanced noiseless cross-phase modulation, Light: Sci. Appl. **1**, e40 (2012).

[22] D. T. Le, W. Asavanant, and N. B. An, Heralded preparation of polarization entanglement via quantum scissors, Phys. Rev. A **104**, 012612 (2021).

[23] Z.-B. Chen, G. Hou, and Y.-D. Zhang, Quantum nonlocality and applications in quantum-information processing of hybrid entangled states, Phys. Rev. A **65**, 032317 (2002).

[24] K. Park, S.-W. Lee, and H. Jeong, Quantum teleportation between particlelike and fieldlike qubits using hybrid entanglement under decoherence effects, Phys. Rev. A **86**, 062301 (2012).

[25] H. Kwon and H. Jeong, Violation of the Bell–Clauser-Horne-Shimony-Holt inequality using imperfect photodetectors with optical hybrid states, Phys. Rev. A **88**, 052127 (2013).
[26] S.-W. Lee and H. Jeong, Near-deterministic quantum teleportation and resource-efficient quantum computation using linear optics and hybrid qubits, Phys. Rev. A **87**, 022326 (2013).
[27] U. L. Andersen, J. S. Neergaard-Nielsen, P. van Loock, and A. Furusawa, Hybrid discrete and continuous-variable quantum information, Nat. Phys. **11**, 713 (2015).
[28] S. Omkar, Y. S. Teo, and H. Jeong, Resource-efficient topological fault-tolerant quantum computation with hybrid entanglement of light, Phys. Rev. Lett. **125**, 060501 (2020).
[29] S. Omkar, Y. S. Teo, S.-W. Lee, and H. Jeong, Highly photon-loss-tolerant quantum computing using hybrid qubits, Phys. Rev. A **103**, 032602 (2021).
[30] S. Bose and H. Jeong, Quantum teleportation of hybrid qubits and single-photon qubits using Gaussian resources, Phys. Rev. A **105**, 032434 (2022).
[31] M. He and R. Malaney, Teleportation of hybrid entangled states with continuous-variable entanglement, Sci. Rep. **12**, 17169 (2022).
[32] Y.-B. Sheng, L. Zhou, and G.-L. Long, Hybrid entanglement purification for quantum repeaters, Phys. Rev. A **88**, 022302 (2013).
[33] Y. Lim, J. Joo, T. P. Spiller, and H. Jeong, Loss-resilient photonic entanglement swapping using optical hybrid states, Phys. Rev. A **94**, 062337 (2016).
[34] H. Jeong, A. Zavatta, M. Kang, S.-W. Lee, L. S. Costanzo, S. Grandi, T. C. Ralph, and M. Bellini, Generation of hybrid entanglement of light, Nat. Photonics **8**, 564 (2014).
[35] O. Morin, K. Huang, J. Liu, L. H. Jeannic, C. Fabre, and J. Laurat, Remote creation of hybrid entanglement between particle-like and wave-like optical qubits, Nat. Photonics **8**, 570 (2014).
[36] A. E. Ulanov, D. Sychev, A. A. Pushkina, I. A. Fedorov, and A. I. Lvovsky, Quantum teleportation between discrete and continuous encodings of an optical qubit, Phys. Rev. Lett. **118**, 160501 (2017).
[37] D. V. Sychev, A. E. Ulanov, E. S. Tiunov, A. A. Pushkina, A. Kuzhamuratov, V. Novikov, and A. I. Lvovsky, Entanglement and teleportation between polarization and wave-like encodings of an optical qubit, Nat. Commun. **9**, 3672 (2018).
[38] T. Darras, B. E. Asenbeck, G. Guccione, A. Cavaillès, H. Le Jeannic, and J. Laurat, A quantum-bit encoding converter, Nat. Photonics **17**, 165 (2023).
[39] B. Qi, P. Lougovski, R. Pooser, W. Grice, and M. Bobrek, Generating the local oscillator "locally" in continuous-variable quantum key distribution based on coherent detection, Phys. Rev. X **5**, 041009 (2015).
[40] P. Jouguet, S. Kunz-Jacques, A. Leverrier, P. Grangier, and E. Diamanti, Experimental demonstration of long-distance continuous-variable quantum key distribution, Nat. Photonics **7**, 378 (2013).
[41] M. Zou, Y. Mao, and T.-Y. Chen, Rigorous calibration of homodyne detection efficiency for continuous-variable quantum key distribution, Opt. Express **30**, 22788 (2022).
[42] G. Zhang, J. Y. Haw, H. Cai, F. Xu, S. M. Assad, J. F. Fitzsimons, X. Zhou, Y. Zhang, S. Yu, J. Wu, W. Ser, L. C. Kwek, and A. Q. Liu, An integrated silicon photonic chip platform for continuous-variable quantum key distribution, Nat. Photonics **13**, 839 (2019).
[43] Y. Zhang, Z. Chen, S. Pirandola, X. Wang, C. Zhou, B. Chu, Y. Zhao, B. Xu, S. Yu, and H. Guo, Long-distance continuous-variable quantum key distribution over 202.81 km of fiber, Phys. Rev. Lett. **125**, 010502 (2020).
[44] While a photon-number-resolving detector measures the number of photons detected, an ON-OFF detector indicates only whether a photon is detected or not detected. As a consequence, an ON-OFF detector is much less demanding than a photon-number-resolving detector. Recent advances in technology have led to the development of single-photon detectors with efficiencies as high as 0.84–0.91 [69–71] with the use of a high-contrast grating in nanophotonics settings. This, in turn, implies that the efficiency of an ON-OFF detector can be safely approximated as being up to 0.80 (if not more).
[45] C.-W. Lee and H. Jeong, Quantification of macroscopic quantum superpositions within phase space, Phys. Rev. Lett. **106**, 220401 (2011).
[46] J. S. Neergaard-Nielsen, Y. Eto, C.-W. Lee, H. Jeong, and M. Sasaki, Quantum tele-amplification with a continuous-variable superposition state, Nat. Photonics **7**, 439 (2013).
[47] H.-K. Lo, M. Curty, and B. Qi, Measurement-device-independent quantum key distribution, Phys. Rev. Lett. **108**, 130503 (2012).
[48] S. Pirandola, C. Ottaviani, G. Spedalieri, C. Weedbrook, S. L. Braunstein, S. Lloyd, T. Gehring, C. S. Jacobsen, and U. L. Andersen, High-rate measurement-device-independent quantum cryptography, Nat. Photonics **9**, 397 (2015).
[49] S. L. Braunstein and S. Pirandola, Side-channel-free quantum key distribution, Phys. Rev. Lett. **108**, 130502 (2012).
[50] H.-L. Yin, T.-Y. Chen, Z.-W. Yu, H. Liu, L.-X. You, Y.-H. Zhou, S.-J. Chen, Y. Mao, M.-Q. Huang, W.-J. Zhang, H. Chen, M. J. Li, D. Nolan, F. Zhou, X. Jiang, Z. Wang, Q. Zhang, X.-B. Wang, and J.-W. Pan, Measurement-device-independent quantum key distribution over a 404 km optical fiber, Phys. Rev. Lett. **117**, 190501 (2016).
[51] H. Kwon and H. Jeong, Generation of hybrid entanglement between a single-photon polarization qubit and a coherent state, Phys. Rev. A **91**, 012340 (2015).
[52] S. Li, H. Yan, Y. He, and H. Wang, Experimentally feasible generation protocol for polarized hybrid entanglement, Phys. Rev. A **98**, 022334 (2018).
[53] S. A. Podoshvedov and N. B. An, Designs of interactions between discrete and continuous-variable states for generation of hybrid entanglement, Quantum Inf. Process. **18**, 68 (2019).
[54] K. Huang, H. L. Jeannic, O. Morin, T. Darras, G. Guccione, A. Cavaillès, and J. Laurat, Engineering optical hybrid entanglement between discrete- and continuous-variable states, New J. Phys. **21**, 083033 (2019).
[55] J. Wen, I. Novikova, C. Qian, C. Zhang, and S. Du, Hybrid entanglement between optical discrete polarizations and continuous quadrature variables, Photonics **8**, 552 (2021).
[56] J. Singh and V. Mittal, Deterministic generation of hybrid entangled states using quantum walks, ArXiv:2311.02419.

[57] W. Li, L. Zhang, Y. Lu, Z.-P. Li, C. Jiang, Y. Liu, J. Huang, H. Li, Z. Wang, X.-B. Wang, Q. Zhang, L. You, F. Xu, and J.-W. Pan, Twin-field quantum key distribution without phase locking, Phys. Rev. Lett. **130**, 250802 (2023).

[58] Y.-L. Tang, H.-L. Yin, Q. Zhao, H. Liu, X.-X. Sun, M.-Q. Huang, W.-J. Zhang, S.-J. Chen, L. Zhang, L.-X. You, Z. Wang, Y. Liu, C.-Y. Lu, X. Jiang, X. Ma, Q. Zhang, T.-Y. Chen, and J.-W. Pan, Measurement-device-independent quantum key distribution over untrustful metropolitan network, Phys. Rev. X **6**, 011024 (2016).

[59] S. Wehner, D. Elkouss, and R. Hanson, Quantum internet: A vision for the road ahead, Science **362**, eaam9288 (2018).

[60] H.-L. Yin, Y. Fu, H. Liu, Q.-J. Tang, J. Wang, L.-X. You, W.-J. Zhang, S.-J. Chen, Z. Wang, Q. Zhang, T.-Y. Chen, Z.-B. Chen, and J.-W. Pan, Experimental quantum digital signature over 102 km, Phys. Rev. A **95**, 032334 (2017).

[61] W. Zhao, R. Shi, J. Shi, P. Huang, Y. Guo, and D. Huang, Multibit quantum digital signature with continuous variables using basis encoding over insecure channels, Phys. Rev. A **103**, 012410 (2021).

[62] B. D. M. Jones, I. Šupić, R. Uola, N. Brunner, and P. Skrzypczyk, Network quantum steering, Phys. Rev. Lett. **127**, 170405 (2021).

[63] https://doi.org/10.13039/501100011033.

[64] S. M. Barnett, D. T. Pegg, and J. Jeffers, Equivalence of a lossless beam splitter and a nondegenerate parametric amplifier in conditional measurements, Opt. Commun. **172**, 55 (1999).

[65] K. Życzkowski, P. Horodecki, A. Sanpera, and M. Lewenstein, Volume of the set of separable states, Phys. Rev. A **58**, 883 (1998).

[66] M. B. Plenio, Logarithmic negativity: A full entanglement monotone that is not convex, Phys. Rev. Lett. **95**, 090503 (2005).

[67] F. Grosshans, N. J. Cerf, J. Wenger, R. Tualle-Brouri, and P. Grangier, Virtual entanglement and reconciliation protocols for quantum cryptography with continuous variables, Quantum Inf. Comput. **3**, 535 (2003).

[68] C. Ottaviani, G. Spedalieri, S. L. Braunstein, and S. Pirandola, Continuous-variable quantum cryptography with an untrusted relay: Detailed security analysis of the symmetric configuration, Phys. Rev. A **91**, 022320 (2015).

[69] W. Pernice, C. Schuck, O. Minaeva, M. Li, G. Goltsman, A. Sergienko, and H. Tang, High-speed and high-efficiency travelling wave single-photon detectors embedded in nanophotonic circuits, Nat. Commun. **3**, 1325 (2012).

[70] C. Wei, W. Wang, D. Liu, M. Gu, and X. Wu, High-efficiency and large light-receiving area superconducting nanowire single-photon detector integrated with high-contrast grating, Photonics Res. **9**, 2253 (2021).

[71] S. Miki, S. Miyajima, F. China, M. Yabuno, and H. Terai, Photon detection at 1 ns time intervals using 16-element SNSPD array with SFQ multiplexer, Opt. Lett. **46**, 6015 (2021).